

https://dspace.org/

Insulated conductor covers for vulture protection on power lines

Chitungo, Givemore

2013-02-11
http://hdl.handle.net/10539/12413

Downloaded from a DSpace repository. https://dspace.org/

INSULATED CONDUCTOR COVERS FOR VULTURE PROTECTION ON POWER LINES

Givemore Chitungo

A research report submitted to the Faculty of Engineering and Built Environment, University of the Witwatersrand, in partial fulfilment of the requirements for the degree of Master of Science in Engineering

Johannesburg, 2012

Table of Contents

DECLARATION....3
ACKNOWLEDGEMENT....4
ABSTRACT....5
LIST OF FIGURES....6
LIST OF TABLES....7
LIST OF SYMBOLS....8
1 The research overview.... 9
1.1 Introduction 9
1.2 Problem Statement 10
1.3 Knowledge to be gained 11
1.4 The research methodology 12
1.5 Research report structure 12
2 The research problem 14
2.1 Introduction 14
2.2 Insulated conductor covers and HV line insulators 14
2.3 Identification of bird electrocution hotspots for the case study 15
2.4 Novelty 18
2.5 Research hypothesis 18
2.6 Leakage current equivalent circuit model 19
2.6.1 Surface resistance 20
2.7 Vulture electrical model 21
2.8 Sparkover circuit model 22
2.9 Concluding remarks 23
3 Electric fields and gap sparkover 24
3.1 Introduction 24
3.2 Sparkover in small air gaps 24
3.3 Standard electrode gaps 26
3.3.1 Atmospheric correction factors 26
3.3.2 Sparkover voltage for rod-rod gaps 28
3.3.3 Rod-plane geometry 30
3.3.4 Conductor-rod geometry 31
3.4 Predicting the sparkover voltage 32
3.5 Concluding remarks 33

4 The hydrophilic polymeric insulator flashover process 34
4.1 Introduction 34
4.2 Polluted insulator flashover 34
4.2.1 Drybands and dry-band arcing 35
4.3 Critical leakage current and voltage 36
4.3.1 Surface leakage currents 37
4.4 Predicting flashover 39
4.4.1 Critical leakage current 41
4.4.2 Critical voltage 44
4.5 Concluding remarks 45
5 Experimental investigation 47
5.1 Introduction 47
5.1.1 Pollution monitoring techniques 47
5.2 Experimental Procedure 48
5.3 Pollution mixture concentration 50
5.3.1 Surface conductivity 51
5.3.2 Measuring surface conductivity 52
5.3.3 Surface conductivity measurement results 54
5.3.4 Conductivity test result analysis 56
5.3.5 Limitation of the test method 58
5.4 Flashover stress and leakage current experimental results 59
5.5 Discussion 60
5.6 Concluding remarks 60
6 Conclusion 62
REFERENCES 64
BIBLIOGRAPHY 66
APPENDICES 69

Declaration

I declare that this research project is my own unaided work. It is being submitted for the Degree of Master of Science in Engineering to the University of the Witwatersrand Johannesburg. It has not been submitted before for any degree or examination to any other University

_____

_____Day of_____Year_____

Abstract

Overhead power lines are among the top contributors to vulture mortalities in South Africa due to direct contact electrocution. Furthermore these electrocution incidences on the endangered birds affect the power quality and the power reliability. Utilities around the world, faced with the same problem, have implemented various solutions such as reconfiguring the lines to bird-friendly structures, retrofitting the existing structures and making use of underground cable by-passes. The choice of these preventative measures is a function of cost and reliability. This research presents a case study involving insulated conductor covers that were retrofitted on 88 kV power line structures to mitigate vulture electrocutions. This research report presents a theoretical evaluation of the performance of the insulated conductor covers together with laboratory tests performed to evaluate the theoretical predictions. These results conclude that the insulated conductor cover flashover performance is similar to that of High voltage (HV) insulators however it requires a lower specific creepage distance to prevent flashover for any corresponding pollution severity level.

Acknowledgements

I would to like thank everyone who inspired and encouraged me to complete my research project.

To God, thank you for the strength and determination without which I would have lost hope.

To my supervisor, Dr John van Coller, thank you for all your crucial advice.

To my co-supervisor, Dr Cuthbert Nyamupangedengu, thank you for being always around for encouragement and guidance throughout the research project.

To my wife and family, thank you for your love and patience.

List of Figures

Figure 2-1: Insulated conductor cover (the conductor (not shown) passes through the center of the above) 15
Figure 3-1: Variation of sparkover voltage with gap spacing for rod-rod geometry [16] 29
Figure 3-2: Variation of sparkover voltage of rod-plane gap with gap spacing [17] 31
Figure 4-1: Variation of current and dry-band width with applied voltage [20] .. 35
Figure 4-2: Dry band and arc discharge development on a polluted surface 36
Figure 4-3: Measured leakage current waveforms for kaolin-salt polluted insulator sample under clean fog at 20 kV [22] 38
Figure 4-4: The proposed electrical equivalent circuits [22] 38
Figure 5-1: Experimental Set-up:1. HV bushing step up transformer, 2. Voltage divider, 3. Polluted insulated conductor cover, 4. Leakage current meter, 5. Multimeter, 6. Series resistance 49
Figure 5-2: Electrical representation of experimental Set-up 50
Figure 5-3: Surface resistivity test setup: 1.Variac, 2. Multimeter 1, 3.Polluted polymeric sheet, 4. Multimeter 2 5. Series resistor 53
Figure 5-4: Electrical representation of the surface conductivity test set up 54
Figure 5-5: Voltage distribution across Sample 1 and series resistor for wet and dry pollution layer 55
Figure 5-6: Voltage distribution across Sample 2 and series resistor for wet and dry pollution layer 56
Figure 5-7: Leakage current on clean vs. polluted insulated conductor cover measured at position P1 59

List of Tables

Table 2-1: IEC surface resistivity classification [8]..... 20
Table 3-1: Values of exponent, *m* and *w* as a function of parameter g [15] 28
Table 5-1: An extract of conductivity measurements of different kaolin pollutant solutions from [23]..... 51
Table 5-2: Surface conductivity for sample sheets polluted with a Kaolin-NaCl solution with concentration of 40 g-10 g per litre of distilled water..... 58
Table 5-3: Voltage vs. Leakage current at different contact position along the insulator surface 59

List of symbols

Resistance	R [ohm]
Conductivity	σ [μS]
Capacitance	C [F]
Impedance	Z [Ω]
Townsend's secondary ionisation coefficient	γ [mm^{-1}]
Townsend's primary ionisation coefficient	α [mm^{-1}]
Townsend's primary attachment coefficient	η [mm^{-1}]
Electric field strength	E [V/m]
Gas pressure	p [Torr]
Conductor irregularity factor	m [unitless]
Relative air density	δ [unitless]
Form factor	F [unitless]
Voltage	V [Volts]
Gap distance	d [cm]

1 THE RESEARCH OVERVIEW

1.1 Introduction

Power lines span several thousands of kilometres across South Africa to deliver electricity to homes and industries. Power lines unfortunately sometimes interfere with nature - electrocutions and collisions are amongst the greatest threats that vultures as well as other birds of prey face in Southern Africa [1]. Although the more recently built power line structures are vulture friendly, earlier designs have resulted in the death of many vultures. These birds are electrocuted when they touch simultaneously two live conductors or a live conductor and an earthed part of the pylon [2].

In South Africa, bird-unfriendly structures, notably steel lattice structures, are still found in the North West province where these migratory birds breed. The utility, in partnership with an environmental conservationist, is conducting research in order to understand the negative interaction of the vultures with the power lines to introduce effective mitigation measures. The conservationist employed by the utility acts as a watchdog reporting any incidences on the power lines.

Incidences of voltage dips and conductors breaking due to flashovers resulting from contact electrocution are being reported. This continued threat to the vulture population as well as the system reliability has created a significant concern for both the utility and the conservationist. The utility in South Africa in collaboration with the conservationist has been proactive and identified problem locations which have been found to be mainly in wetlands and game reserves. Mitigation strategies have therefore been targeted at these specific areas.

The main problem in these areas is birds perching on power lines to rest or to spot their prey and in the process bridging the safety clearances. In line with other utility practices, reconfiguration of structures, use of underground cable bypasses and retrofitting existing structures are the options available for mitigating these

adverse effects [3]. These mitigation measures do not only assist with minimising vulture electrocutions but also improve the power system reliability.

The utility, identifying the high capital cost requirement of the first two options, opted for the third option. To date it has targeted the identified hotspots and installed bird guards (retrofits installed on power line structures to prevent birds from perching) and also pilot insulated conductor covers on the portions of the conductor directly below the structures.

1.2 Problem Statement

The option of insulating the conductors is effective in protecting the birds against direct contact electrocution more so when insulation with an earthed screen is used. This technique allows the birds to make contact with the power line without any danger of electrocution or electrostatic shock. The insulated conductor covers currently installed do not have an earthed screen thus rendering the vulture susceptible to static discharge shock when close to the cover. This technique has generally succeeded in reducing cases of vulture electrocutions although additional problems have been introduced. These problems are:

1. Tracking which occurs on the insulated conductor covers due to pollution and insufficient creepage distance.

2. Conductor corrosion which occurs on the portion of the conductors enclosed by the insulated conductor covers.

This research will focus on the first problem with an aim to evaluate the flashover performance of the installed insulated conductor cover when contact at various locations along its surface is made with the vulture sitting on an earthed steel structure. A technical explanation for the electrocution incidences that have been reported on these mitigated locations is required to help propose modifications to the insulated conductor cover to enhance its flashover performance.

The second problem stated above, while having a major impact on the success of this mitigation technique, is out of the scope of this investigation. It is being researched concurrently with the former as a related project. Insulated conductors together with bare conductors are intended to be installed in a natural coastal environment for a period of 24 months to evaluate the corrosion performance. Bare conductors will be installed for control purposes. The corrosion status of the conductors will be evaluated every six months. It is hypothesised that the insulated conductor cover can potentially corrode the conductor by creating humid conditions inside the cover during rainy seasons thereby reducing the life expectancy of the conductors.

1.3 Knowledge to be gained

Power line retrofits available in the market, used for electrocution prevention, come in many non-standard shapes and sizes with the choice being guided by the insulation level of the product. This is mainly because there are many different tower structures that are in use by utilities around the world making it difficult to develop a product that can be used on all tower structures. Utilities therefore have to look for the best-fit product that addresses their identified concerns.

This research will add to the knowledge of the analysis techniques that can be used before any roll-out. Utilities will save a lot of money by avoiding installation of products that may not fully address all the issues.

An in-depth knowledge of the level of mitigation achieved by these insulating cover retrofits will equip the utilities with sufficient motivation to opt for more effective solutions such as tower structure reconfiguration and underground cable by-passes even though these would require huge capital costs. Elsewhere in the world environmental laws to protect migratory birds from the dangers of power lines have been passed and this has resulted in some utilities being fined amounts of the order of USD 100,000 for violating these laws [4]. In South Africa the current Environmental Impact Assessment (EIA) Regulation provides for protection of migratory birds on new installations only; however increased

pressure from conservationists may see this regulation being extended to existing structures.

1.4 The research methodology

The insulated conductor cover under investigation is designed to avoid high voltage bus-bar flashover as a result of direct contact with birds, squirrels and other wildlife [5]. The utility has adapted this cover to protect vultures against direct contact with the bare overhead conductor while sitting on an earthed steel structure.

When the insulated conductor cover is used in this manner, it assumes a function similar to that of a high voltage insulator at the instant there is contact with a vulture. It is thus reasonable to apply the same principles for evaluating the flashover performance of high voltage insulators to the insulated conductor cover. The following methodology is therefore used:

1. Standard rod-rod gap breakdown voltages (standard atmospheric conditions and square-cut electrodes) are used to predict breakdown in the gap created by the approaching vulture wing tip modelled as an earthed rod at various positions in the vicinity of the insulated conductor cover.
2. An equivalent circuit for surface flashover of the insulated conductor cover is developed which represents vulture contact at various positions along the surface.
3. A laboratory experiment is set up to test the surface flashover predictions.

1.5 Research report structure

The research report has six chapters. Each chapter describes different components of the research that builds up to the conclusion of the investigation.

Chapter 1: This chapter gives an introduction to the research work, defines the problem and then presents the proposed research methodology.

Chapter 2: This chapter gives a background to the methods used to gather information leading to the choice of mitigation measure as well as justifying this option. Parameters required for critical analysis of the insulated conductor cover are also identified. The flashover performance in relation to creepage distance and gap geometry is discussed. Limitations to the research methodology are also discussed.

Chapter 3: This chapter analyses and predicts the breakdown voltage of the gap created when the vulture wing tip is at various positions in the vicinity of the insulated conductor cover. The breakdown voltage is predicted from the breakdown voltage of standard rod-rod gaps.

Chapter 4: This chapter discusses the flashover processes on polluted polymeric insulators and applies these concepts to the insulated conductor cover when a vulture makes direct contact while sitting on the earthed structure. An equivalent circuit of a polluted insulator is then used to predict flashover over the surface of the insulated conductor cover at various points of contact.

Chapter 5: In this chapter a laboratory experiment consisting of application of high voltage between the phase conductor and various earth contact positions along the surface of the insulated conductor cover is described - each time noting the flashover voltage. The experimental results are then compared with the theoretical predictions.

Chapter 6: In this chapter the conclusions are presented and also recommendations proposed to help in further advancing the effectiveness of the electrocution mitigation approach under investigation.

2 THE RESEARCH PROBLEM

2.1 Introduction

In addition to bird streamer problems on steel lattice tower structures, contact electrocution has been suspected to be responsible for the continued vulture electrocutions. The former has been mitigated by use of bird guards, whereas for the latter, insulated conductor covers have been proposed. Pilot insulated conductor covers have been installed in the identified problem areas. This research focuses on evaluating insulated conductor cover performance.

2.2 Insulated conductor covers and HV line insulators

High voltage (HV) line insulators are used for conductor support and for insulating the earthed tower structure hardware from the live conductors. An insulated conductor cover is used to prevent external objects such as wildlife from coming into direct contact with the live conductors. While both HV line insulators and insulated conductor covers provide insulation functions, the former additionally requires sufficient mechanical strength.

Figure 2-1 shows a sketch of the insulated conductor cover. It is a hollow cylindrically shaped object made from a 2 mm thick hydrophilic polymeric material with a relative permittivity of 5. This material has similar properties to that of hydrophilic polymeric insulators and it is assumed that the flashover processes of the two products are similar. The only differences between the two are that:

1. The HV line insulator is connected between the live conductor and earth whereas the insulated conductor cover surrounds the live conductor only.
2. Leakage currents on a polluted line insulator flow continuously whereas on the insulated conductor cover leakage currents flow only when there is contact with an external earthed object.

3. Leakage current flows over the entire surface of the insulator whereas on insulated conductor covers the leakage current flows only over a portion of the surface area where contact is made.

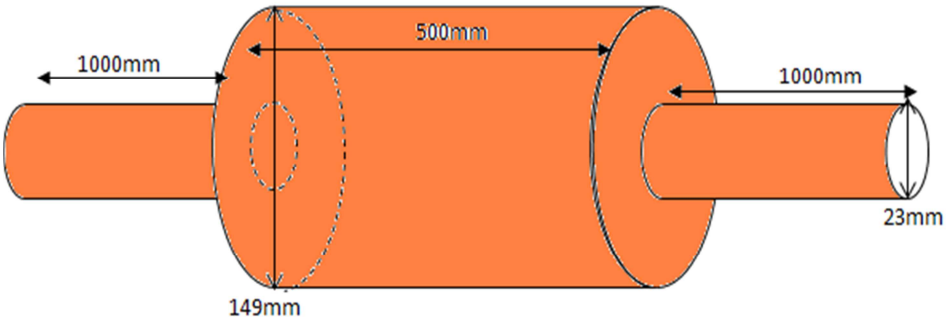


Figure 2-1: Insulated conductor cover (the conductor (not shown) passes through the center of the above)

The insulated conductor cover is moulded into a hollow cylinder of different radii as shown in Figure 2-1. The middle section has a larger radius to accommodate the conductor-insulator connection accessories whereas the outer sections have a smaller radius to allow the insulated conductor cover to fit snugly on the conductor.

2.3 Identification of bird electrocution hotspots for the case study

The faults recorded on the utility power line of interest during the period 2005 to 2007 by a numerical protection relay located in the feeding substation were used to identify bird electrocution hotspots are shown in Figure 2-2.

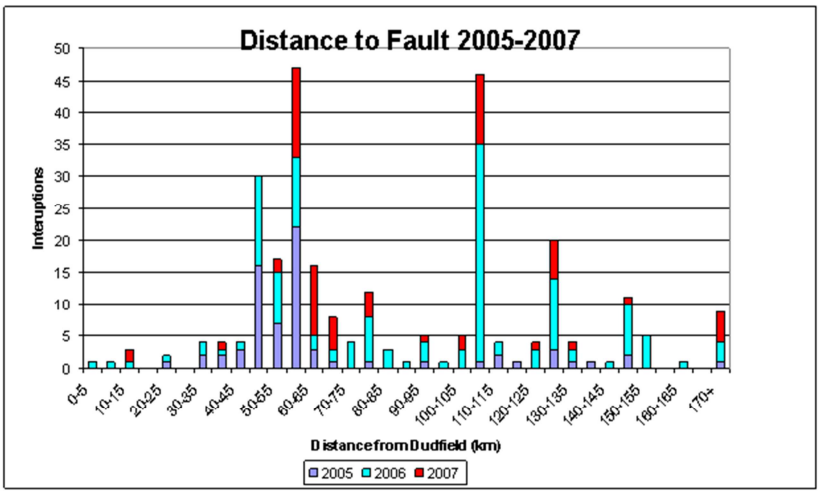


Figure 2-2: Faults recorded on a steel lattice tower structure power line [6].

The fault distribution in Figure 2-2 shows that the line portion between 55 km and 75 km from the substation is a hotspot area. The faults in this location were correlated with known bird outage characteristics to extract possible contact incidences.

All faults recorded between 2300 hrs and 0600 hrs with successful auto-reclose and no obvious alternative causes such as lightning, contamination and switching were extracted. It was found that the red outer phase recorded a relatively high number of these faults when compared to other phases. The position and the presence of bird guards on the outer phase made it highly susceptible to contact electrocution incidences and therefore the power utility made a decision to install insulated conductor covers on the red outer phase.

.

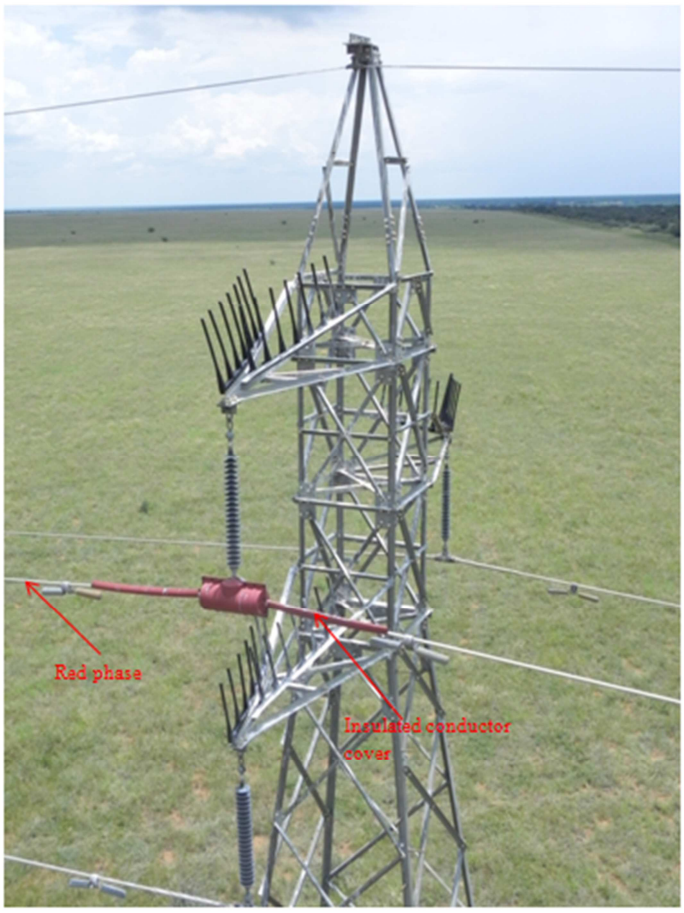


Figure 2-3: Photo showing an insulated conductor cover installed on a lattice tower structure [6].

Figure 2-3 shows a steel lattice tower structure configuration with an insulated conductor cover installed to mitigate vulture direct contact electrocution. The structure also has the bird guards installed, these were initially installed to prevent vultures from perching directly above the HV insulator as well as directly below the red phase conductor to prevent streamers and contact electrocution respectively. However due to the forceful nature of the vultures these birds tend to force their way through the bird guards which results in accidental contact with the live conductor. Insulated conductor cover prevents electrocution in case of this accidental contact.

2.4 Novelty

The insulated conductor cover under investigation commonly used on substation busbar and equipment bushings was adapted for use on overhead power lines. This practice is novel and to the best knowledge of the author, no work has ever been done to analyse the flashover performance of this product when utilised on overhead power lines to prevent direct contact electrocution.

2.5 Research hypothesis

A vulture in contact with or in close proximity to the insulated conductor cover shown in Figure 2-3 gives rise to the development of surface leakage current and perhaps surface discharges. The extent of these two components is critical to effective prevention of vulture electrocutions. The hypothesis is illustrated in Figure 2-4.

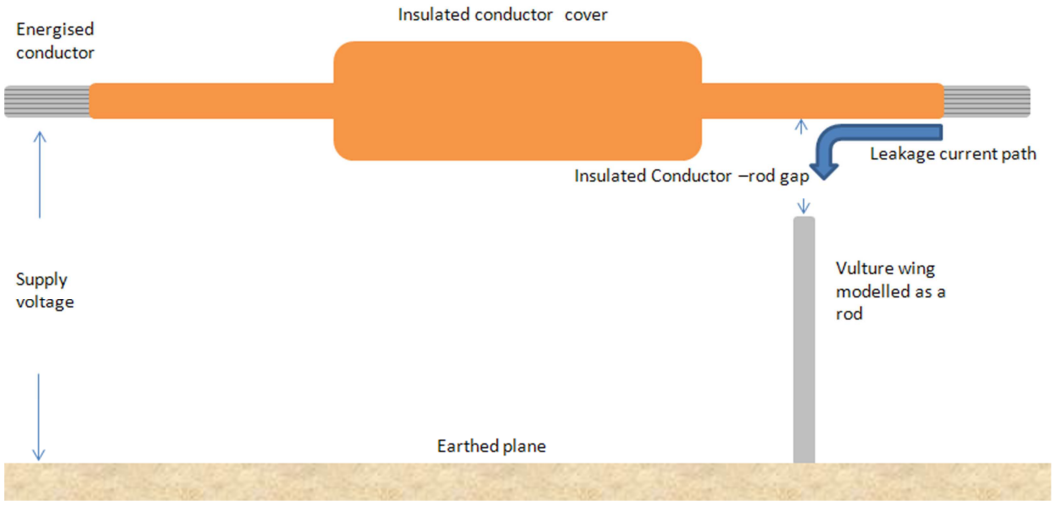


Figure 2-4: Illustration of the hypothesised flashover condition

It is hypothesised that if the insulated conductor cover-rod gap sparks over or if the vulture makes contact with the insulated conductor cover at a point where there is insufficient creepage distance to the energised conductor, high leakage currents will flow that may lead to surface flashover and electrocution of the vulture.

Equivalent circuits shown in Figure 2-5 and 2-7 electrically represent sparkover conditions as well as estimate the leakage current magnitude to test the hypothesis. If proved correct, the equivalent circuits will be used to modify the insulated conductor cover design by varying the parameters until a surface condition unfavourable to flashover is achieved.

2.6 Leakage current equivalent circuit model

Figure 2-5 shows a proposed equivalent circuit representing the condition at the instant the vulture makes contact with the insulated conductor cover on a conductor with voltage V_s. At this instant the leakage current through the bird resistance R_B is limited by the parallel combination of the surface resistance R_s and insulation impedance Z_T, The latter consists of capacitance C_T and resistance R_T of the insulated conductor cover material.

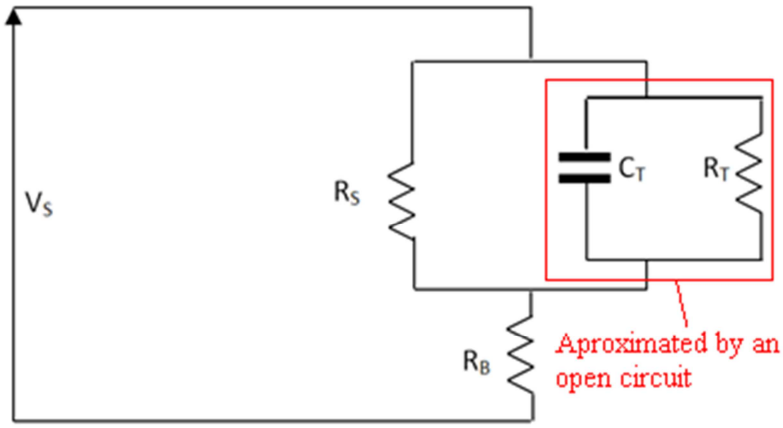


Figure 2-5: Leakage current equivalent circuit

It has been observed on the power line in question that flashover normally occurs in the early hours of the morning in the presence of dew or rain. For these conditions the insulation surface is wet resulting in the surface resistance R_s being relatively small compared to the insulation impedance $Z_{T;}$ therefore most of the leakage current flows over the insulation surface. The research assumes that the insulation impedance is infinitely high and is represented as an open circuit. The

effective resistance becomes a series combination of the surface resistance and vulture resistance.

2.6.1 Surface resistance

Holtzhausen [7] showed that the surface resistance of a cylindrically shaped object with a film of uniform pollution can be calculated using equation 2-1

$$R = \frac{L}{2\pi r \sigma_s} \qquad 2\text{-}1$$

Where

L is the length of the cylindrical surface [mm]

r is the radius of the polluted cylinder [mm]

σ_s is the surface layer conductivity [µS]

The International Electrotechnical Commission (IEC) [8] specifies the pollution level on the insulators based on the severity of the pollution that will be expected to accumulate on the surface. This is quantified by the conductivity of the pollution and is specified in Table 2-1

Table 2-1: IEC surface resistivity classification [8]

IEC Pollution Classification	**Surface layer conductivity (µS)**
Light	15-20
Medium	24-30
Heavy	>30

This research assumes light pollution which corresponds to a surface layer conductivity of 20µS. The resultant surface resistance of the insulated conductor cover obtained by substituting in Equation 2-1 is approximately 1.45 MΩ.

In practice a vulture makes contact with a small portion of the insulated conductor cover surface. The effective surface resistance is therefore much higher than the

value calculated above. The surface leakage current path to earth is through this high resistance, small contact surface area.

2.7 Vulture electrical model

The vulture type common in South Africa stands 1.1 m high with a wing span of about 2.55 m and weighs between 7 kg and 9.5 kg [9]

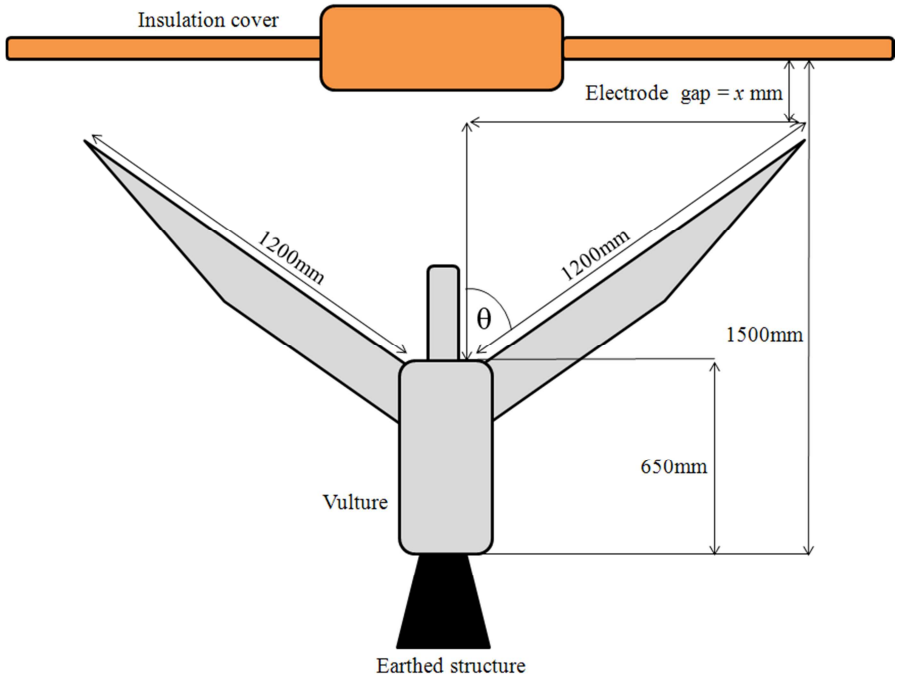


Figure 2-6: Model of a vulture sitting on an earthed structure with wings spread out.

Figure 2-6 shows a vulture model with it wings spread out such that it creates a conductor-rod gap geometry. It is assumed that the vulture can span its wings up to an angle θ=45° and the gap can be of the order of 0.2 cm. The wing tip is represented as a hemispherical rod with a diameter of 20 cm

Nelson [10] in his unpublished document showed that wet feathers burn off at around 7 kV whereas dry feathers can withstand up to 70 kV when in contact with a live conductor. The time of the day when most of the electrocutions occur coincides with the time for the morning dew. It is therefore assumed that the

vulture will be wet and the vulture resistance for the equivalent circuit can be calculated in this condition.

Considering that when the vulture makes contact with the insulated conductor cover the resultant surface leakage current is of the order of milliamps, this author assumed the vulture resistance R_B to be 1000 Ω. The value was selected so that the corresponding voltage drop across resistance R_B is of the order of volts and hence easily measured by a conventional analogue voltmeter enabling an accurate determination of the surface leakage current. This estimate does not affect the flashover leakage current since the estimated resistance value is relatively small compared to the series surface resistance of the insulated conductor cover (1.45 MΩ) calculated in section 2.6.1.

2.8 Sparkover circuit model

Figure 2-7 shows the proposed equivalent circuit diagram representing conditions hypothesised in Figure 2-4. A non-uniform electric field stress E is developed in the insulated conductor cover-rod gap. The wet insulated conductor cover is modelled as a plane at a high voltage and the vulture wing tip is modelled as an earthed rod.

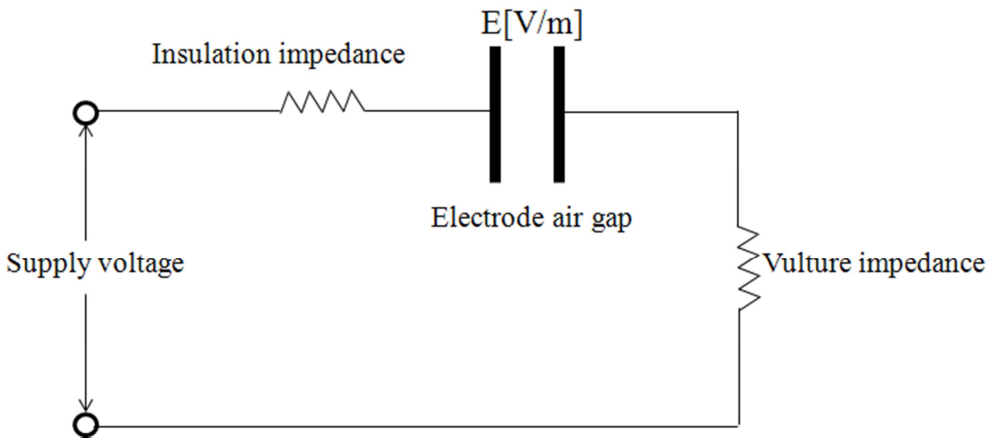


Figure 2-7: Equivalent circuit for air breakdown.

Localised discharges are developed on the wing tip where points of highest field intensity exist and these may develop into a complete sparkover. The discharge current flowing during sparkover is limited by the insulation surface resistance.

The electric field distribution depends on the gap geometry and is independent of electrode material. Non-uniformity of electric field in this geometry makes it difficult to accurately determine the sparkover voltage. Standard rod-rod electrode gap sparkover voltages are thus used to estimate the sparkover in the gap.

2.9 Concluding remarks

The leakage current and discharge current are estimated under wet conditions. This approach is valid as

1. The vulture contact with the insulation is momentary and may not allow the surface to form dry bands.
2. Flashover is common under wet polluted conditions.
3. The insulation material is hydrophilic and therefore exhibits lower surface resistivity when wet.
4. The vulture feathers are conductive when wet; otherwise they are highly resistive hence rendered non-conductive in this research.

The estimated insulated conductor cover surface resistance of 1.45 MΩ (in practice much higher because the leakage current does not flow uniformly round the cylinder) is used to predict the leakage current at the instant of the contact. At this point the surface is wet and the resistance is linear, otherwise it varies non-linearly with voltage [11].

The next chapter discusses breakdown of the rod-plane gap created when the vulture is simulated at different positions in the vicinity of the insulated conductor cover. The breakdown in this gap is analysed assuming standard rod-rod gap breakdown is applicable.

3 ELECTRIC FIELDS AND GAP SPARKOVER

3.1 Introduction

If the electric field developed in an air gap is sufficiently large, ionisation of the air may arise which may result in sparkover across the air gap. A vulture sitting on the earthed steel tower structure with its wings spanned towards the insulated covered conductor is assumed to constitute a conductor-rod gap geometry where the gap length is less than 10 cm. It is assumed that the vulture wing is spread out at an angle such that the electric field is concentrated at the wing tip. This condition may result in the development of corona discharges at the wing tip that can transform into a sparkover.

The sparkover voltage of small gaps can be accurately predicted by numerical solution of the Townsend and Meek equations at low pressures and high pressures respectively. Use of these breakdown models in this case is limited due to the lack of fundamental data such as the field distribution in complex geometries. As a result of this limitation, this research uses data available in the literature for the standard rod-rod sparkover voltages to predict sparkover when the vulture wing tip approaches the insulated conductor cover.

3.2 Sparkover in small air gaps

The sparkover voltage across air gaps depends highly on the gap geometry which determines the field distribution. Generally for the same gap length and atmospheric conditions, the breakdown voltage in non-uniform fields is always lower than that in uniform fields. The reason for the lower breakdown voltage in non-uniform fields is essentially because of the electric field enhancement that initiates avalanches at voltages lower than for uniform fields

Typically, the Townsend mechanism applies for *pd* products less than 1000 torr-cm, or for gaps lengths around a centimeter at one atmosphere, while for longer gap lengths up to 100 cm at any pressure the streamer mechanism applies.

Townsend's breakdown involves the development of a succession of sufficiently sized electron avalanches that reach the opposite electrode, while streamer breakdown involves the development of a sufficiently sized single electron avalanche that develops into a conducting plasma channel that reaches the opposite electrode.

An electron avalanche increases exponentially in size as a result of ionizing collisions. Reather [12] showed that an avalanche is required to reach a critical value of 10^8 for sparkover to occur. Equation 3-1 represents the avalanche growth across the gap.

$$n(x) = e^{\alpha x} \qquad 3\text{-}1$$

Where

α is the Townsend's primary ionisation coefficient [mm^{-1}]

$n(x)$ is the number of electrons at a distance x for the cathode [unitless]

x is the distance from the cathode [mm]

The Townsend breakdown criteria states that the critical condition for breakdown is achieved when equation 3-2 is satisfied.

$$\gamma(e^{\alpha d} - 1) = 1 \qquad 3\text{-}2$$

Where

γ is the Townsend's secondary ionisation coefficient [mm^{-1}]

d is the gap length [mm]

Townsend's secondary ionisation coefficient is very sensitive to electrode condition and gas impurities, which can only be accurately defined under laboratory conditions.

The streamer breakdown criterion states that breakdown occurs when equation 3-3 is satisfied.

$$\int_0^{\mathrm{d}} \alpha \, dx = 20 \qquad 3\text{-}3$$

It is apparent that the breakdown voltage prediction by both criteria depends on Townsend's coefficients. Field measurement by various researchers [13] showed

that the Townsend's primary coefficients are a function of the electric field intensity and pressure for a specific temperature. These are constant in uniform fields and vary in non-uniform fields. To calculate the sparkover voltage across an electrode gap it is thus essential to accurately compute the electric field distribution for the geometry.

In the absence of accurately known field distributions, such as in the gap in this investigation, standard rod-rod sparkover voltages are used to predict sparkover.

In that regard the rest of the sections in this chapter presents how the standard rod-rod sparkover voltage is used to predict the insulated conductor cover-vulture sparkover voltage.

3.3 Standard electrode gaps

The sparkover voltages of standard rod-rod and rod-plane gap geometries are linear for a limited range of atmospheric conditions and gap lengths. These electrode gap geometries, even though not accurately representing configurations such as the conductor-rod geometry, give an acceptable estimation for sparkover voltages for practical gaps less than 25 cm [14]. The standardised sparkover voltages are specified for standards atmospheric conditions at a temperature 20˚C, absolute pressure 1.013bar and absolute humidity 11gm^{-3}. For non-standard conditions the values are corrected to standard conditions. Conversely standard values can be corrected to any prevailing atmospheric condition.

3.3.1 Atmospheric correction factors

The atmospheric correction factor is proportional to the product of the air density correction factor k_1 and the humidity correction factor k_2 [15]. This is given by Equation 3-4

$$K_t = k_1 k_2 \qquad 3\text{-}4$$

Where K_t is the atmospheric correction factor [unitless]

The sparkover voltage V_h corrected for atmospheric conditions is therefore given by Equation 3-5

$$V_h = K_t V_0 \qquad 3\text{-}5$$

The air density correction factor is obtained from the relative air density by the relationship $k_1 = \delta^m$. The exponent *m* is specified in [15] for specific ranges of g as shown in table 3-1. The value of *m* ranges between 0 and 1. The relative air density given in equation 3-6

$$\delta = \frac{\mathrm{P}}{\mathrm{P_0}} . \frac{(273+\mathrm{T_0})}{(273+\mathrm{T})} \qquad 3\text{-}6$$

Where

P is the atmospheric pressure [kPa]

T is the temperature [˚C]

P_0 is equal to 101.3kPa

T_0 is equal to 20˚C

The air density correction factor is further shown in [15] to be reliable for $0.8 < k_1 < 1.05$. This is applicable to the current investigation since the relative air density is expected to vary marginally within the standard temperature and pressure.

The a.c sparkover voltage humidity correction factor is given by $k_2 = k^w$ where *k* is obtained from Equation 3-7. The humidity correction factor is valid for $1 \geq h/\delta \leq 13\mathrm{gm}^{-3}$. The exponent *w* in the humidity correction factor is also specified in [15] as shown in table 3-1 for the specific ranges of g.

$$k = 1 + 0.012\left(\frac{h}{\delta} - 11\right) \qquad 3\text{-}7$$

Where

h is the absolute humidity [gm^{-3}]

The exponents in the air density and humidity correction factors discussed above depend on gap length and relative air density and absolute humidity as shown in Table 3-1

Table 3-1: Values of exponent, *m* and *w* as a function of parameter g [15]

$g = \frac{U_{50}}{500L\delta k}$	m	w
< 0.2	0	0
0.2 to 1.0	$g\,(g - 0.2)/0.8$	$g\,(g - 0.2)/0.8$
1.0 to 1.2	1.0	1.0
1.2 to 2.0	1.0	$(2.2 - g)\,(2.0 - g)/0.8$
> 0.2	1.0	0

From Table 3-1 the value of *g* applicable to the investigation lies between 1 and 2, the exponents' *m* and *w* are hence assumed to be equal to 1. This implies that the air density and humidity correction factors are approximated by the Equation 3-6 (δ) and Equation 3-7 (*k*) respectively.

It is however important to note that although the relative air density δ has an influence on the value of the humidity correction factor; it is the absolute humidity that is of greater importance as this has been experimentally shown in [17] to have a wider variation when compared to the corresponding relative air density. The air density correction factor is therefore ignored in this investigation

3.3.2 Sparkover voltage for rod-rod gaps

The sparkover voltages of standard rod-rod gaps are documented in the literature for both d.c. voltages and peak values of power frequency a.c. voltages. The gap consists of two rods mounted on a common axis with the ends cut at right angles to the axis. These brass rods have a square cross-section with side between 15mm and 25mm. The rod length is chosen such that it is equal to or greater than one-half of the gap spacing [16].

It is shown in [16] that the sparkover voltage V_0 [kV], for a square electrode at standard atmospheric conditions varies linearly with gap length and is given by

$$V_0 = 2 + 534d \qquad 3\text{-}8$$

Where

d is gap length [m]

Figure 3-1 shows the variation of the a.c. and the d.c. sparkover voltages as a function of gap length for a rod-rod geometry at standard atmospheric conditions. The a.c. voltage curve in Figure 3-1 was redrawn from the rod-rod sparkover voltage data obtained in [16] whereas the d.c. sparkover voltage was obtained from Equation 3-4.

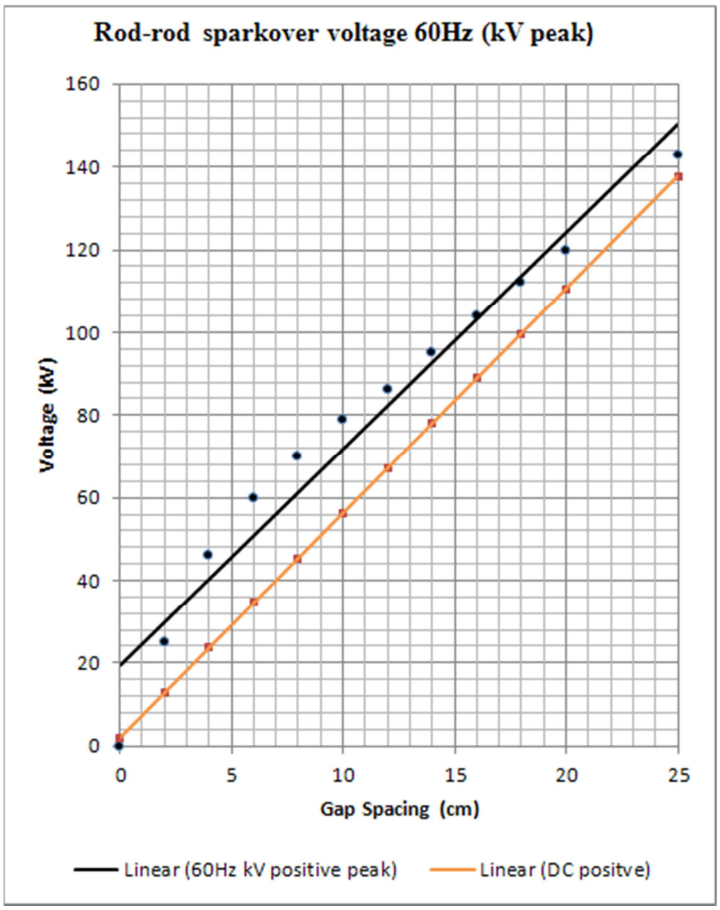


Figure 3-1: Variation of sparkover voltage with gap spacing for rod-rod geometry [16]

Figure 3-1 shows that in both cases the variation of sparkover voltage with gap spacing for rod-rod geometries is linear and as expected the sparkover for the a.c. voltage is always higher than that of the d.c. voltage.

3.3.3 Rod-plane geometry

The geometry consists of a rod with the same dimensions as in the rod-rod geometry vertically suspended over a plane sheet. The dimension of the plane sheet is chosen such that all gap flashovers occur within its surface area.

The sparkover voltage of this gap geometry is linear over a wider range of absolute humidity compared to the rod-rod geometry. The sparkover voltage was shown in [14] through a series of experiments to be always lower than that of the rod-rod gap for all gap lengths. The reason for this is that the field distribution for this geometry is more divergent when compared to that of the rod-rod geometry. This effect becomes more evident when the gap length increases as shown in Figure 3-2 where the difference significantly widens.

The gap geometry was further shown in [17] to possess this linear characteristic for both hemispherical shaped rod tips and square cut rod tips, hence making it a more appropriate sparkover prediction tool when applied to practical gaps found in coastal regions where high humid conditions are common.

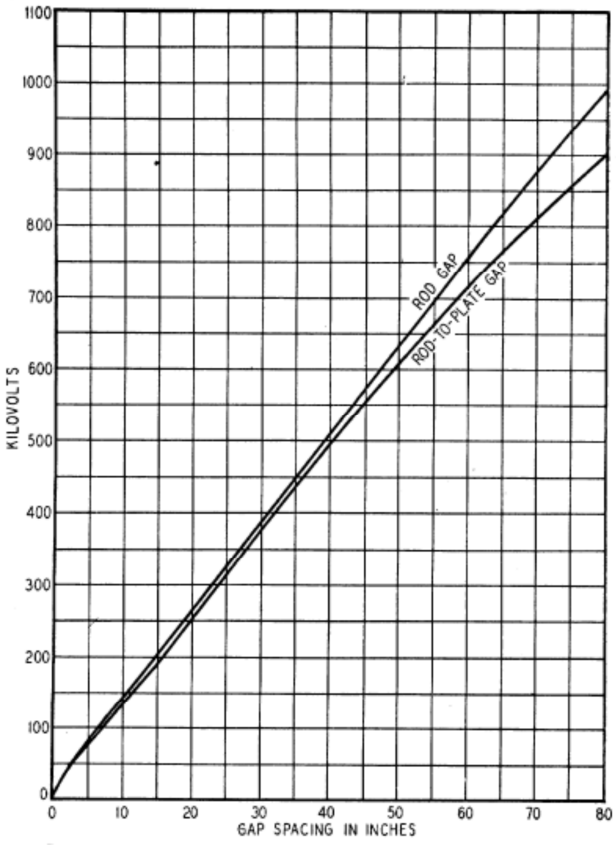


Figure 3-2: Variation of sparkover voltage of rod-plane gap with gap spacing (P.L. Bellaschi 1934:1641) [17]

Figure 3-2 shows that for gap lengths less than 25 cm (10 inches) the flashover voltage of the rod-plane and the rod-rod geometries are the almost the same. This gap length is applicable to the current investigation. It is therefore reasonable to use the standard rod-rod sparkover voltage data to predict breakdown for the insulated conductor cover-rod gap in the current investigation.

3.3.4 Conductor-rod geometry

This geometry is an accurate representation of practical electrode gaps that are found on power lines. Sparkover voltages for this arrangement were experimentally obtained in [18] using various 3 m long conductors (solid and stranded) having various diameters together with an electrode with similar dimension to that in rod-rod and rod-plane arrangements. The experimental results showed that

1. Conductor stranding, sagging and curvature of the conductors do not have significant effect on the sparkover voltage

2. Conductor diameter has a significant effect on the sparkover voltage

It was further shown that the sparkover voltage of the conductor-rod arrangement for small gap lengths is marginally less than that of the standard rod-rod gap whereas for longer gap lengths it is higher.

This further justifies the rationale of using the standard rod-rod gap to predict the sparkover voltage for the gap of interest in this investigation.

3.4 Predicting the sparkover voltage

Discussions in the previous sections on the sparkover voltage for the rod-rod, rod-plane and conductor-rod gap geometries have shown that for small gaps less than 25 cm (applicable to the current investigation), the rod-rod gap sparkover voltage matches accurately the sparkover voltage experienced between the conductor insulation cover and the vulture wing tip due to its linearity over a wide range of atmospheric conditions.

The calculated voltage across the insulated conductor cover-vulture wing gap for an 88 kV line is 50.8 kV_{rms} (71.8 kV_{peak}). If standard atmospheric conditions are assumed, the corresponding sparkover length from Figure 3-1 is 10 cm.

For non-standard conditions the humidity correction factor is applied. Assuming that $h/\delta = 1\,\mathrm{gm}^{-1}$ the humidity correction factor calculated from Equation 3-7 is equal to 0.86. The sparkover voltage at non-standard atmospheric conditions calculated from Equation 3 is given by

$$V_0 = \frac{50.8}{0.86} = 59.1\ \mathrm{KV_{rms}}\ \left(83.6\mathrm{KV_{peak}}\right)$$

The corresponding value when $h/\delta = 13\mathrm{gm}^{-3}$ is assumed to be 49.4 kV_{rms} (69.8 kV_{peak})

From Figure 3-1, the sparkover is predicted to occur at a maximum distance of between 8 cm and 12 cm

3.5 Concluding remarks

When a vulture spans its wings it creates a gap with the insulating conductor cover (assuming the conductor cover is covered with conductive pollution) as the other electrode. This gap sparks over at a maximum gap length of between 8 and 12 cm depending on atmospheric conditions when the covered conductor is energised at 50.8kV.

When sparkover occurs, the vulture does not retract itself but involuntarily continues to make contact with the insulated conductor cover. If the horizontal distance at the point of contact is less than the critical creepage length the probability of surface flashover increases. The next chapter discusses this flashover process.

4 THE HYDROPHILIC POLYMERIC INSULATOR FLASHOVER PROCESS

4.1 Introduction

Pollution flashover of ceramic and hydrophilic polymeric high voltage insulators involves the propagation of an arc across the surface coated with a conductive pollution layer. The conductivity of the pollution layer is usually a result of the moistening of a dry pollution layer by fog, moisture or rain. This leads to the flow of leakage current resulting in the formation of dry-bands and dry-band arcing. This surface arcing process then propagates along the insulator surface until it spans the whole insulator [19].

This chapter discusses the flashover process on polluted insulators and then adapts this to predict surface flashovers on insulated conductor covers. The equivalent circuit proposed in Chapter 2 is used to test the hypothesis that insufficient creepage length is the main cause of the flashovers being experienced where insulated conductor covers are used in the field. This is done by simulating the vulture in contact with the insulated conductor cover at various positions along the length of the insulated conductor cover and comparing the resulting leakage current with the threshold current.

4.2 Polluted insulator flashover

Pollution flashover on a high voltage insulator surface is summarised by the following stages:

a) Settling of dry pollutants on the insulator surface
b) Wetting of the dry pollutants thereby forming the conductive layer
c) Flow of leakage current
d) Formation of dry-bands due to the leakage current flow
e) Dry-band arcing across the dry-bands followed by flashover.

It is essential that the initial leakage current flowing on the insulator surface is sufficiently high to initiate the formation of dry bands. A minimum voltage across

the insulator is also required to sustain the dry-band arcing otherwise the flashover process terminates.

4.2.1 Drybands and dry-band arcing

Leakage current flowing through a conductive pollution layer on the surface of an insulator has a heating effect that causes the drying of the conductive layer forming dry-bands. Discharges across these dry-bands are usually extinguished at the zero crossings of the current but may develop into a flashover across the surface [11].

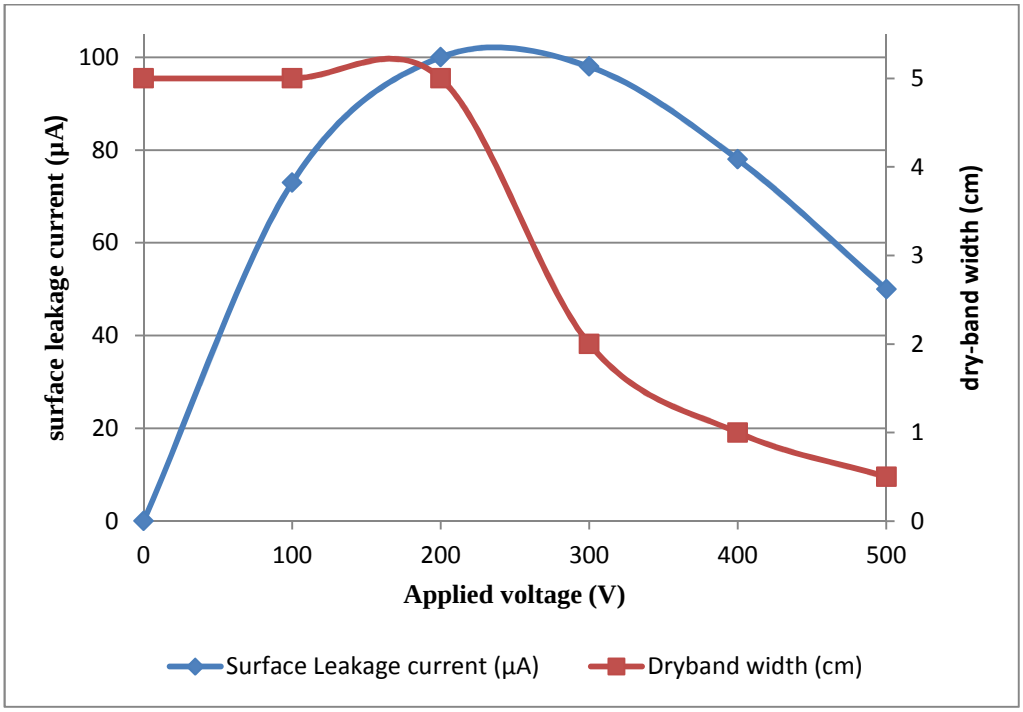


Figure 4-1: Variation of current and dry-band width with applied voltage [20]

Figure 4-1 adopted from [20] shows that the leakage current over the surface of a polluted insulator increases linearly up to a critical voltage where the dry-band formation starts. Beyond this point the surface temperature rises above the ambient causing the moisture in the pollution layer to evaporate - initiating dry-band formation. The high resistance dry band in series with the lower resistance conductive pollution layer causes the voltage to appear mainly across the dry band

(voltage divider effect). At this point non-linearity occurs as a result of the development of arc discharges across these dry-bands. This condition is electrically modelled as a nonlinear resistor in series with the low resistance conductive pollution layer as shown in Figure 4-2.

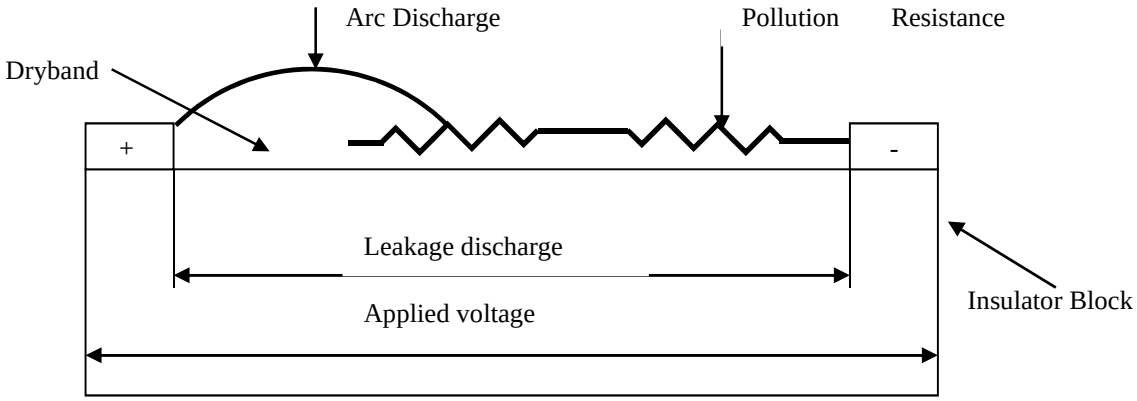


Figure 4-2: Dry band and arc discharge development on a polluted surface

The arc discharge across the dry band in series with the pollution resistance sustains the leakage current. A minimum voltage is required to sustain the arc discharge.

4.3 Critical leakage current and voltage

The previous section showed that a critical voltage and a corresponding critical leakage current are required to complete the insulator surface flashover process. Verma [20] showed that the critical leakage current I_{max} on an insulator surface is determined by Equation 4-1. This assumes an evenly distributed continuous current flowing over the entire insulator surface.

$$I_{max} = \left[\frac{SCD}{15.32}\right]^2 \qquad 4\text{-}1$$

Where

I_{max} is the critical leakage current [mA]

SCD is the Specific Creepage Distance [mm/kV]

In [21] Holtzhausen proposed that the maximum permissible peak leakage current must remain below 0.25 I_{max}. In addition he proposed that the corresponding critical flashover voltage is determined by the empirical Equation 4-2.

$$V_c = k_1 \times 10^{-3} \left[\frac{F \times 10^6}{\sigma_s L} \right]^{k_2} \times L \qquad 4\text{-}2$$

Where:

V_c is the critical flashover voltage [kV]
σ_s is the surface conductivity [μS]
F is the insulator form factor [unitless]
L is the creepage distance [mm]
K_1 is constant equal to 7.6
K_2 is a constant equal to 0.35
Both equations show that the critical flashover value depends on the surface conductivity and insulator form factor.

4.3.1 Surface leakage currents

Surface leakage current flows when a high voltage is applied across a polluted insulator. The leakage current magnitude as shown in the previous section is a function of pollution conductivity. Figure 4-3 shows typical leakage current wave shapes that were measured in [21] on polluted insulator block when a voltage was applied across it. The leakage current waveform displays harmonic current components.

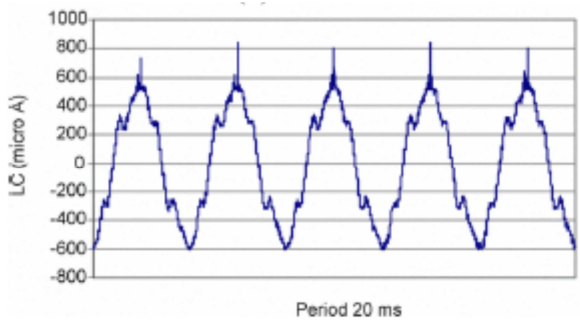


Figure 4-3: Measured leakage current waveforms for kaolin-salt polluted insulator sample under clean fog at 20 kV [22]

An equivalent circuit Figure 4-4 proposed in [22] simulates this leakage current. The circuit is essentially a wet pollution layer with dry-bands in parallel with a clean insulator surface. The wet pollution layer is modelled as a nonlinear resistor Rp and the dry-band as a nonlinear resistor Rdb in parallel with a capacitor Cdb. The clean insulator surface is modelled as a parallel combination of a resistor R1 and a capacitor C1.

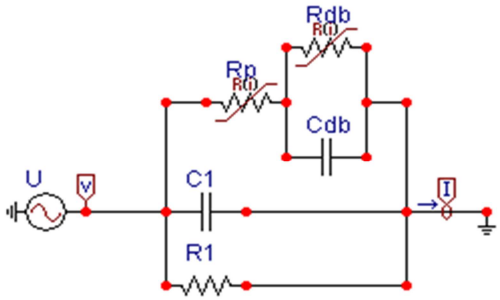


Figure 4-4: The proposed electrical equivalent circuits [22]

The equivalent circuit in Figure 4-4 applies to a polluted hydrophilic polymeric insulator surface. Considering that the insulated conductor cover is made from a similar polymeric material, the equivalent circuit can be extended to this case. The only major differences being that the surface leakage current is momentary and the leakage current path is concentrated over a small contact surface area. Therefore lower total currents are expected to have the same effect as that predicted in Equation 4-1.

4.4 Predicting flashover

Figure 4.5 shows a polluted insulated conductor cover with a total surface length L m. When a vulture sitting on a earthed steel structure makes contact with this insulated conductor cover at a point *x* m from the closest live end, a parallel leakage current path to earth constituting the surface areas corresponding to surface length *x* and L-*x* is created.

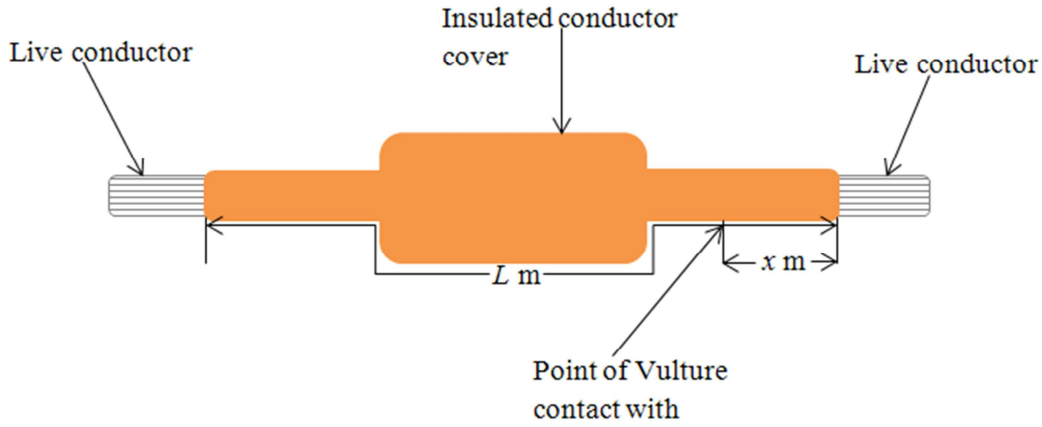


Figure 4-5: Electrical representation of a vulture in contact with a wet insulated conductor cover

Considering that a polluted insulator surface has been shown in the previous section to be electrically represented by the parallel combination of the pollution impedance Z_p and the clean insulation impedance Z_c. The resultant leakage current when a voltage is applied across the insulation has also been shown to be entirely dominated by the pollution conductivity. It is therefore reasonable to represent the insulation impedance in Figure 4-4 with an open circuit. The proposed equivalent circuit can therefore be approximated by the circuit in Figure 4-6

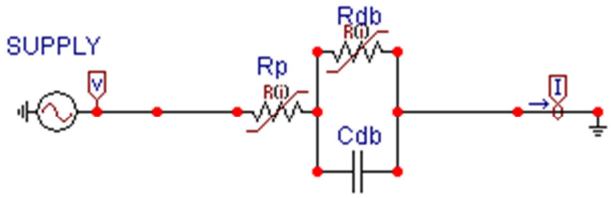


Figure 4-6: Modified equivalent circuit of a polluted insulator

In the case of an insulated conductor cover when the vulture makes contact at point *x*, the surface resistances corresponding to surface lengths (*x*) and (L-*x*) are represented by R_x and R_T-R_x respectively where R_T is the total surface resistance of the insulated conductor cover. Adopting the modified equivalent circuit of Figure 4-6 this scenario is electrically represented in Figure 4-7.

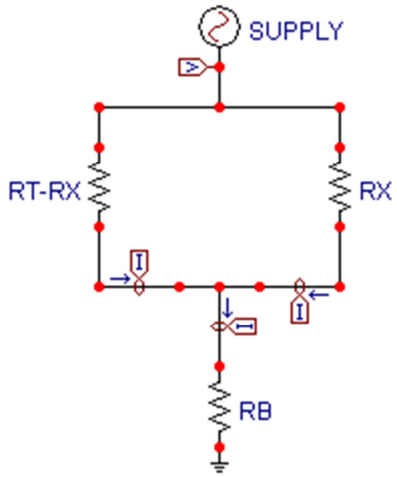


Figure 4-7: Electrical representation of a vulture in contact with a wet insulated conductor cover

The pollution resistances in Figure 4-7 are modelled in their linear range representing the vulture contact. The equivalent circuit simulates the initial current conditions at the point of contact.

With reference to Figure 4-7, when the contact point is midway from either ends of the insulated conductor cover in Figure 4-5 R_x is equal to (R_T - R_x); otherwise it

is always less at all points away from the mid-point. Figure 4-8 shows this variation.

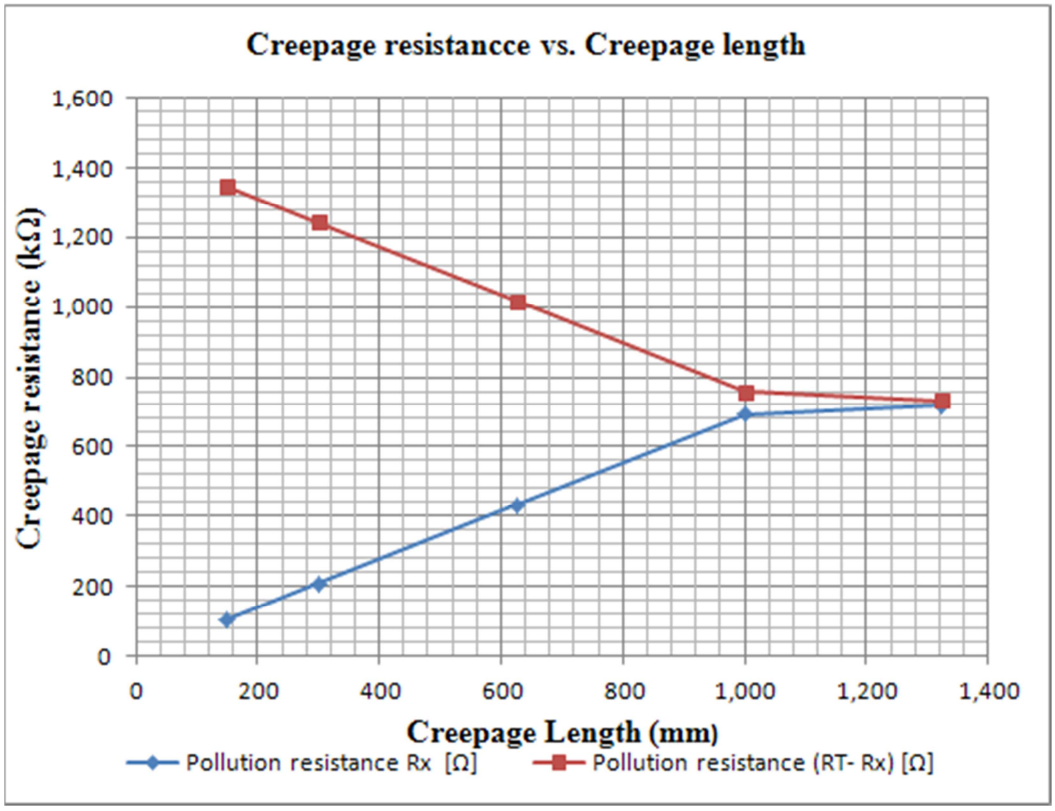


Figure 4-8: Variation of insulated conductor cover surface resistance with creepage length *x*

It is apparent that as the point of contact approaches the live end the difference between R_x and (R_T –R_x) increasing to a point where the total leakage current is entirely determined by R_x. It is at this creepage distance where high probabilities of surface flashover occur.

4.4.1 Critical leakage current

Using the equivalent circuit in Figure 4-7, leakage currents were simulated using the Alternative Transient Program (ATP) program for resistances corresponding to creepage lengths 150 mm, 300 mm, 675 mm, 1000 mm and 1325 mm when voltages 10 kV, 30 kV and 55 kV are applied in turn. The resultant leakage

currents are plotted together with the corresponding threshold current predictions as shown in Figure 4-9.

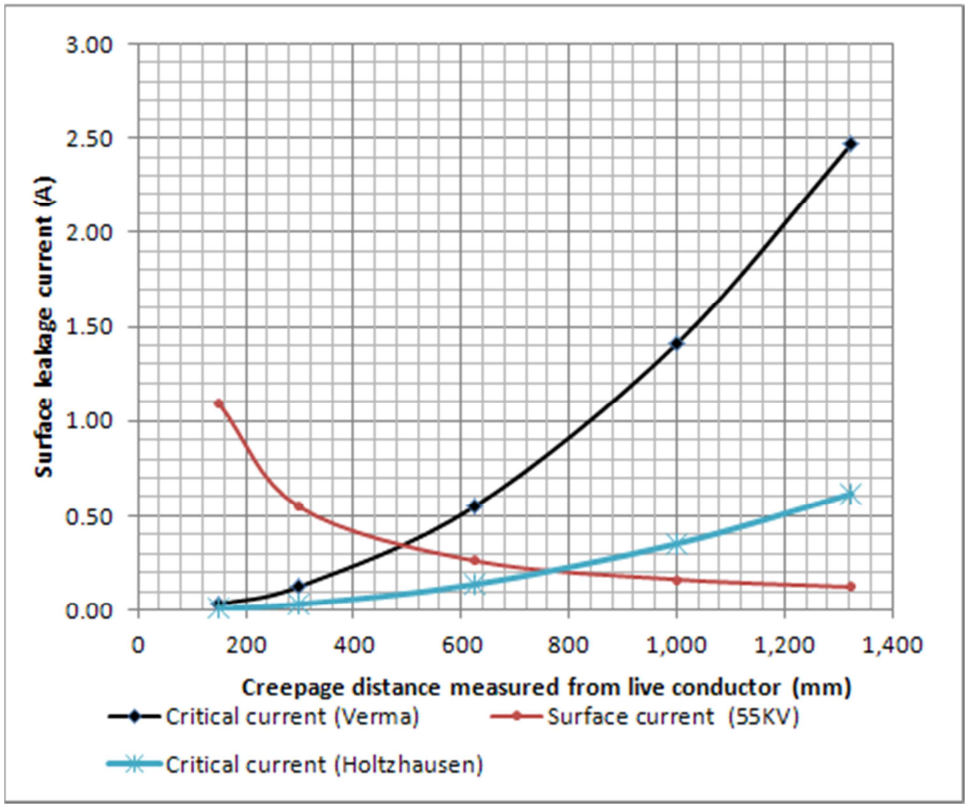


Figure 4-9: Surface leakage current vs. creepage distance with a supply voltage of 55kV

Figure 4-9 shows that when a voltage of 55 kV is applied across the insulated conductor cover, a high probability of flashover occurs when the creepage length is less than 500 mm [I_{max}] and 800 mm [$0.25I_{max}$]. These predictions assume a uniformly distributed continuous leakage current flowing over the entire insulator surface. This is in contrast to current flowing on the insulated conductor cover surface which is concentrated on a small surface area.

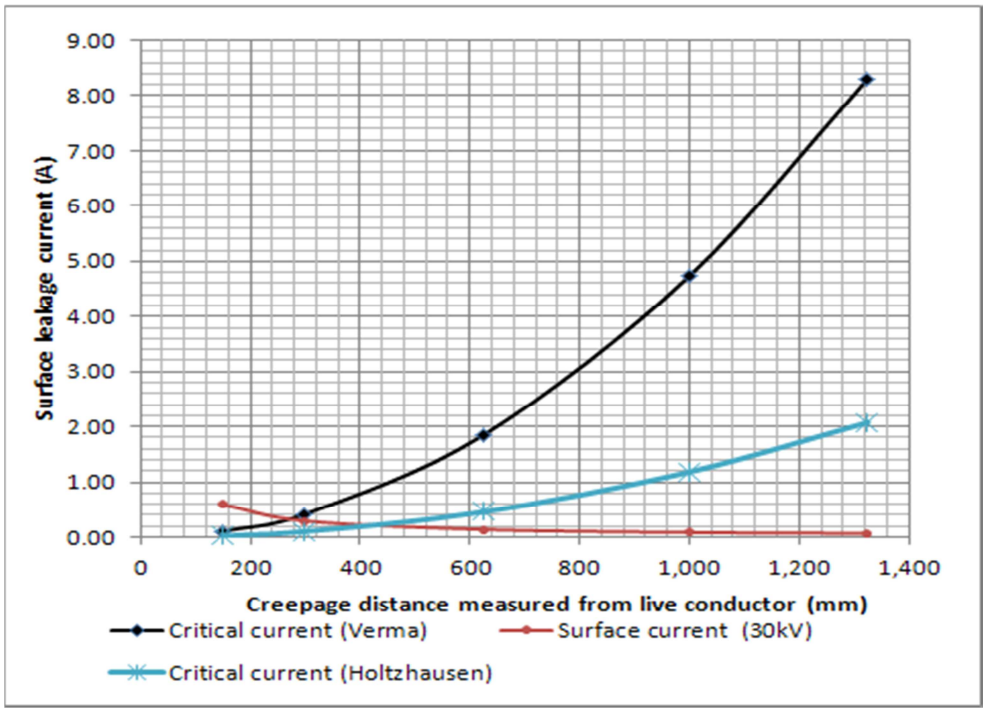


Figure 4-10: Surface leakage current vs. creepage distance for supply voltage of 30 kV

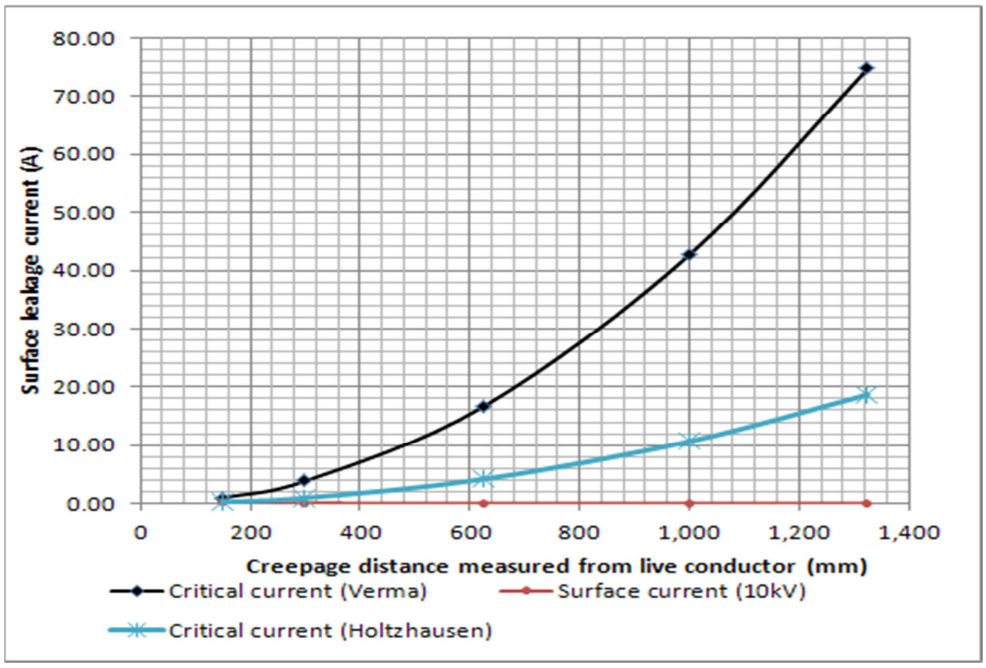


Figure 4-11: Surface leakage current vs. creepage distance for supply voltage of 10 kV

Figure 4-10 and Figure 4-11 shows that when the applied voltage across the insulated conductor cover is reduced, the probability of flashover also reduces as

is predicted to occur at a shorter creepage length. This suggests that flashover voltage is proportional to the creepage length.

4.4.2 Critical voltage

The form factor F of a cylindrical insulator is given by

$$F = \frac{L}{2\pi r} \qquad 4\text{-}3$$

Where

r is radius of the insulator [mm]

Substituting into Equation 4-2 the critical voltage for the insulated conductor cover reduces to Equation 4-4

$$V_c = k_1 \times 10^{-3} \left[\frac{10^6}{2\pi r \sigma_s}\right]^{k_2} \times L \qquad 4\text{-}4$$

For a constant pollution severity the critical voltage varies linearly with creepage length. This is clearly illustrated in Figure 4-12.

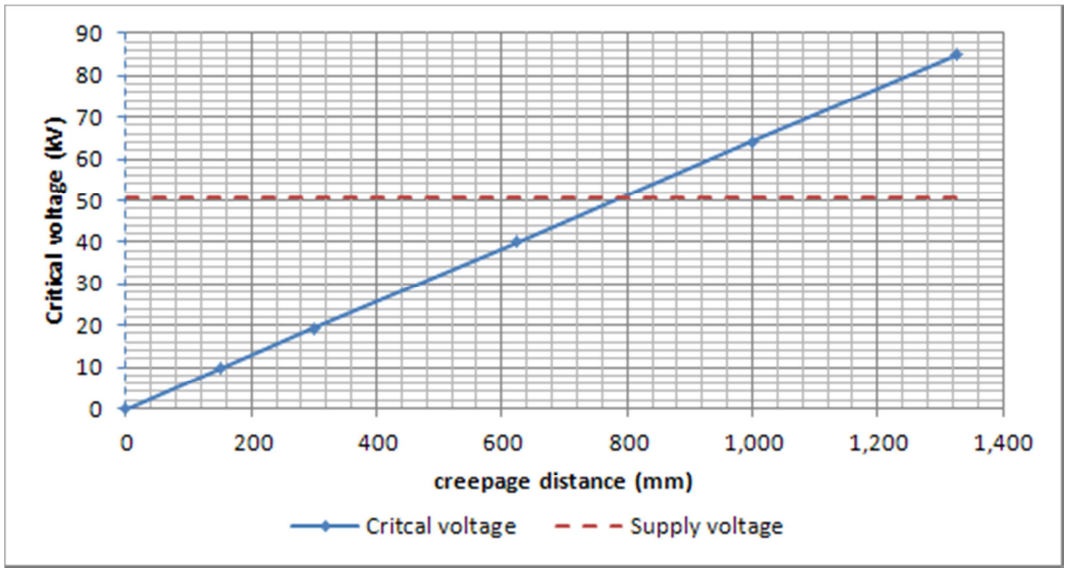


Figure 4-12: Variation of critical voltage with creepage distance

The probability of breakdown increases as the critical voltage falls below the supply voltage. The supply voltage across the insulated conductor cover is a phase-earth voltage of 50.8 kV. Figure 4-12 shows that flashover is likely to occur when the creepage distance is below 800 mm.

The critical creepage distance coincides with that predicted in the equivalent circuit using maximum permissible current ($0.25I_{max}$) proposed in [21] as shown in Figure 4-9. The specific creepage distance at this point is approximately 16 mm/kV which is in line with that recommended in IEC60815-1 for light pollution severity.

4.5 Concluding remarks

Probability of flashover increases if the vulture comes into contact with the insulated conductor cover at a distance less than the critical creepage distance. At this point both the leakage current and the corresponding voltage exceed the threshold values.

- Threshold current and voltage proposed in [21] is used as a reference to predict flashover probabilities for the insulated conductor cover.

- The developed equivalent circuit is used to predict surface flashover by comparing the simulation results with the threshold values calculated from Equation 3-1.

- Creepage length is a critical parameter in the dimensioning of an insulated conductor cover to mitigate surface flashover for a specific pollution severity application.

The flashover process on the insulated conductor cover is similar to that of high voltage insulators. However the leakage current path is concentrated within a small surface area thus requiring a lower total current to have the same effect as that predicted in Equation 3-1.

A laboratory experiment is set up to establish a relationship between the theoretical and the experimental obtained creepage length. This is discussed in the next chapter.

5 EXPERIMENTAL INVESTIGATION

5.1 Introduction

A laboratory experiment was conducted to investigate how insulator surface conditions affect the leakage current as a function of supply voltage and also to determine the flashover voltage as a function of contact position (creepage distance). The latter investigation was performed on a polluted insulated conductor cover.

Theoretical predictions discussed in the previous chapter showed that wet pollution on an insulator surface results in an increased surface leakage current. It was further shown that an insufficient surface creepage length results in flashover.

5.1.1 Pollution monitoring techniques

The previous sections also that surface flashover occurs when the surface current exceeds a maximum value I_{max}. This value is a function of specific creepage distance which in turn is determined by the pollution severity on the insulating surface. In order to determine the flashover performance of an insulator required for a particular application, the following techniques are therefore available for monitoring [25].

1. Measuring of I_{max}
2. Surge counting
3. Flashover stress

The first two options are accurately measure leakage current under controlled environments free from external interference as these involve very low currents in the order of milliamps, whereas the flashover stress technique determines the flashover withstand stress by blowing a fuse rated I_{max} connected in series with the insulation surface. The latter technique is therefore appropriate under the uncontrolled conditions the experiment was conducted

The other acceptable techniques are the measurement of the pollution layer surface conductivity and equivalent salt deposit density (ESDD) measurements. In

these techniques the measured values are compared to pollution severity classifications specified in IEC 815. The standard defines the minimum specific creepage distance required for every pollution severity classification to prevent flashover on an HV insulator in operation

Unlike the case of HV insulators in insulated conductor cover application the leakage current only flows at the instant when there is contact more so and it is concentrated at the point of contact, hence the specific creepage distance in defined in IEC 815 cannot be used directly.

To determine the required specific creepage distance required on insulated conductor cover design, it is thus necessary to measure the flashover stress different points of contact and determine a relationship with well know pollution performance of HV insulators discussed above.

The next section discusses the laboratory experiment set up to measure the insulated conductor cover flashover stress and also to test the theoretical predictions so as to validate the proposed model.

5.2 Experimental Procedure

The tests were performed at room atmospheric conditions with room temperature ($17^{\circ}C$), pressure (0.837 bars) and relative humidity (17%) in the High Voltage Laboratory at the University of the Witwatersrand, Johannesburg. The experiment was set up as shown in Figure 5-1.



Figure 5-1: Experimental Set-up:1. HV bushing step up transformer, 2. Voltage divider, 3. Polluted insulated conductor cover, 4. Leakage current meter, 5. Multimeter, 6. Series resistance

The insulated conductor cover in Figure 5-1 was polluted by pre-depositing a NaCl and kaolin solution mixed in proportions shown in Table 5-1 over the entire surface. The wet pollution was then allowed to dry up as required in the clean fog test; steam was then used to re-wet the pollution by holding the insulated conductor cover over a container of boiling water until the pollution was appropriately wet.

Figure 5-2 shows the electrical representation of the experimental setup of Figure 5-1.

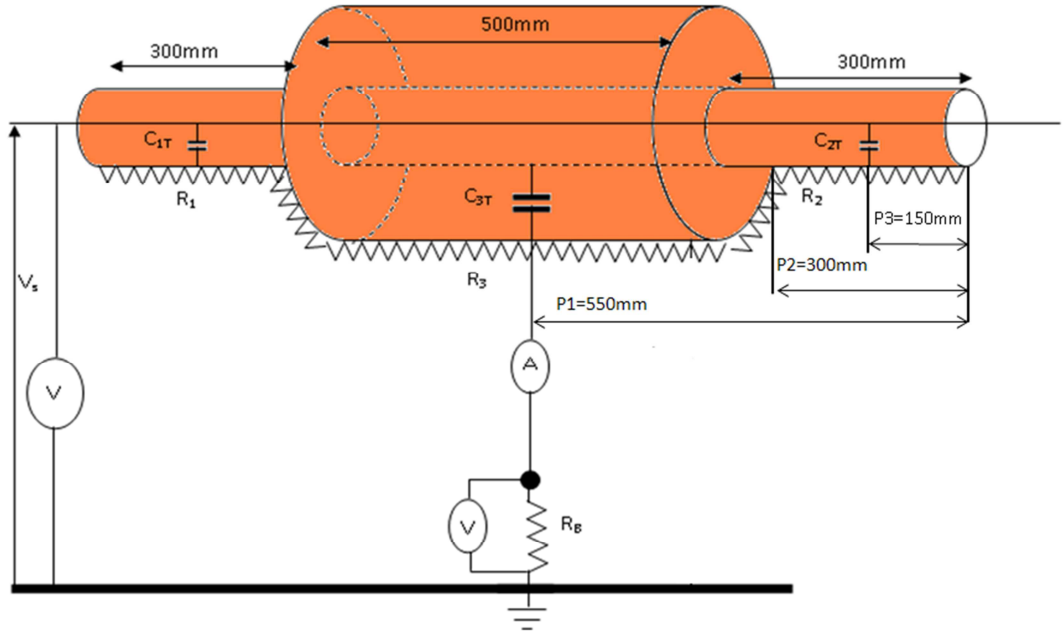


Figure 5-2: Electrical representation of experimental Set-up

In the first tests, voltages ranging from 10 kV to 55 kV which represent voltages within the expected phase-to-ground voltage were applied to the insulated conductor cover. A copper wire connected to earth through a 1000Ω resistor to simulate bird contact was attached at position P1 as shown in Figure 5-2 for a clean insulated conductor cover. The applied voltage and the current through the resistor were noted at each voltage step. The same procedure was repeated for the polluted insulated conductor cover. In the second test the procedure above was repeated for the polluted insulated conductor cover this time at positions P2 and P3 as shown in Figure 5-2.

5.3 Pollution mixture concentration

Table 5-1 below shows the NaCl concentration in g/ltr mixed with 40g of kaolin prepared to simulate pollution and the corresponding solution conductivity.

Table 5-1: An extract of conductivity measurements of different kaolin pollutant solutions from [23]

Pollutant concentration (gr/ltr)	Solution conductivity (μS/cm)
20	16.64
40	17.07
80	21
100	22.7
120	25.3

In the experiment a pollutant concentration of 10 gr/ltr of NaCl was used to simulate light pollution levels defined according to IEC pollution classification shown in Table 2-1.

It was shown in [25] that the measurement of pollution layer conductance is an acceptable technique for assessing the pollution severity on insulator surface. The shortcoming of this method is in addition to the layer pollution severity it also heavily depends on the amount of condensation of the pollution layer.

5.3.1 Surface conductivity

Conductivity is a measure of the ability of a volume of material to allow current to flow per unit length when a voltage is applied across it. If a thin pollution layer with length, width and thickness of L cm, W cm and d cm respectively is pre-deposited on a non-conducting rectangular sheet, the conductivity σ of the pollution layer is determined by Equation 5-1.

$$\sigma = G\frac{L}{\mathrm{d}W} \ [\mathrm{S/cm}] \qquad 5\text{-}1$$

Where

G is the conductance of the pollution layer [S]

Re-arranging Equation 5-1

$$\sigma\mathrm{d} = G\frac{L}{W} \ [S] \qquad 5\text{-}2$$

The term (σd) in Equation 5-2 is defined as the surface conductivity σ_s.

To determine the surface conductivity of the pollution layer pre-deposited on the insulated conductor cover using the NaCl-Kaolin solution in Table 5-1, surface conductance of a polluted sheet with known area dimensions polluted in a similar way to the insulated conductor cover is determined by measuring the voltage drop across the sheet and its corresponding current.

In this research two polymeric sheet cut from the polymeric material similar to that of the insulated conductor cover with length and width dimensions of 60 mm x 65 mm and 105 mm 112 mm respectively. Both sheets are each in turn polluted with kaolin/NaCl concentration of 40 g/10 g and 40 g/40 g per litre of distilled water as shown in table 5-1 using the procedure described above specified in IEC 60507. The dimensions of the sheet are chosen such that the L/W ratio is similar.

5.3.2 Measuring surface conductivity

Figure 5-3 shows the experimental set up to determine the pollution conductivity. In the experiment AC voltage ranging from 0 to 90 V in steps of 10V is applied across the polluted sheet under dry and wet conditions each time noting the voltage across a series resistor. The applied voltage is chosen such that the pollution does no dry up during measurement hence remaining in its linier range, also the series resistance is chosen so that the resultant voltage drop across it is in order of volts.

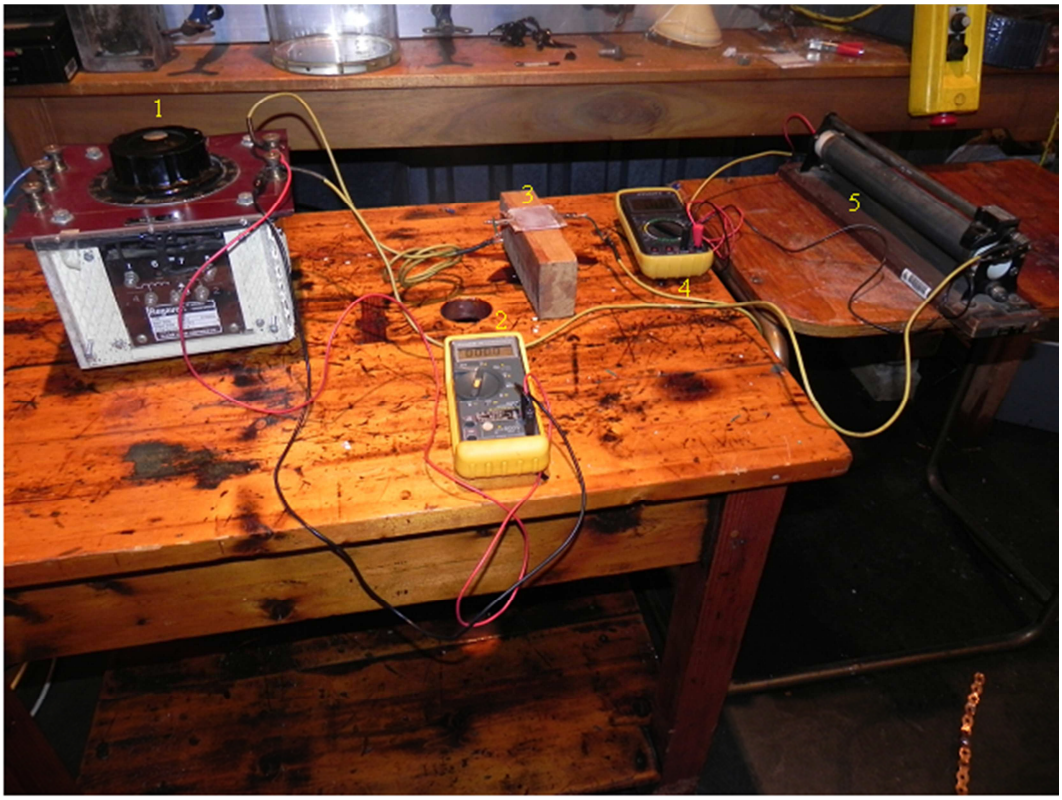


Figure 5-3: Surface resistivity test setup: 1.Variac, 2. Multimeter 1, 3.Polluted polymeric sheet, 4. Multimeter 2 5. Series resistor

Figure 5-4 is the electrical representation of Figure 5-3. The pollution layer is represented as a non-linear resistor in parallel with the sample sheet surface resistance. In this experiment the measurements are done in the linear range of the pollution layer resistance by ensuring that the pollution layer does not up creating dry bands.

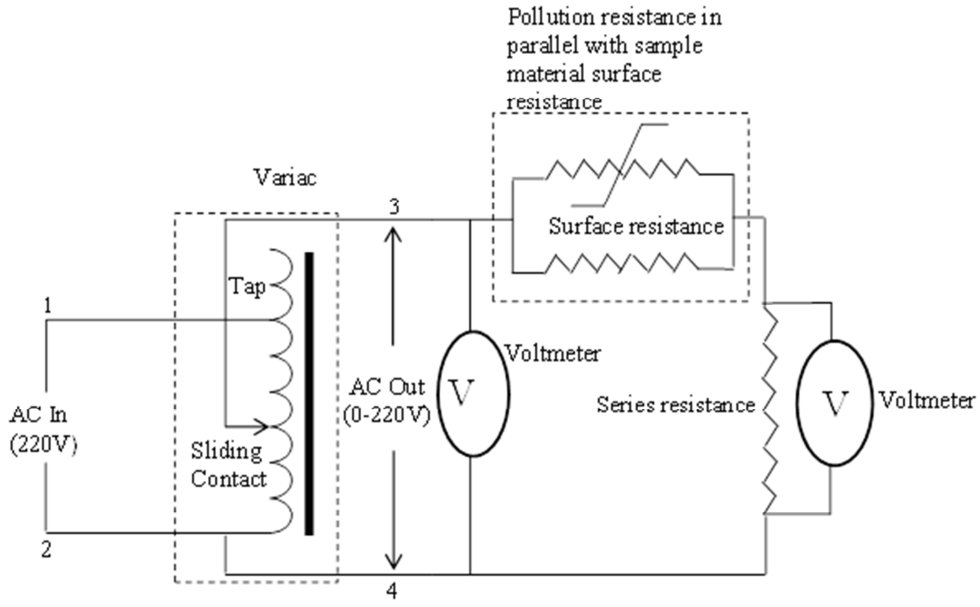


Figure 5-4: Electrical representation of the surface conductivity test set up

It is assumed that the pollution layer is non-conductive when dry and conductive when wet.

5.3.3 Surface conductivity measurement results

Figure 5-5 and Figure 5-6 shows the resultant voltage distribution across the samples 1 and sample 2 plotted against the series resistance when a voltage ranging from 0 to 90 V is applied. In both cases the voltage was applied when the pollution layer was dry as well as wet for the Kaolin/NaCl pollutant with concentration 40 g/10 g and 40 g/40 g.

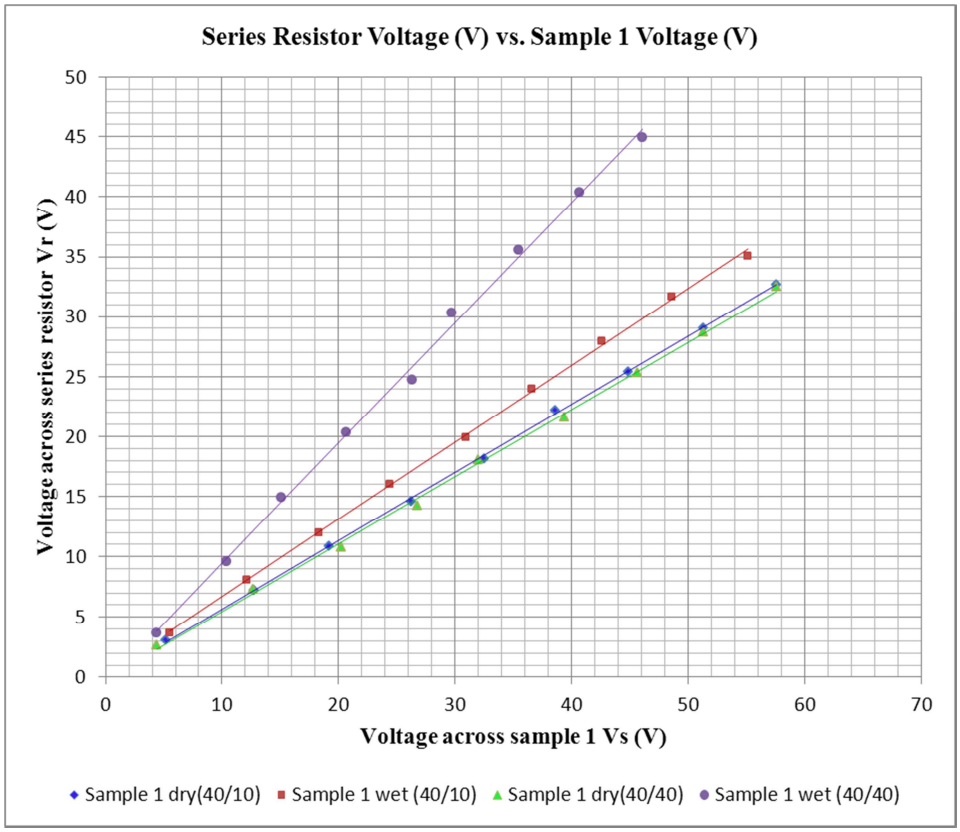


Figure 5-5: Voltage distribution across Sample 1 and series resistor for wet and dry pollution layer

The surface resistance for both pollution levels is under dry condition is the same as expected, this agrees with the assumption that dry pollution is non-conductive. In this case the effective surface resistance is that of the polymeric material otherwise the pollution layer provides a less resistive parallel path.

Surface conductance is dependent on the pollution severity. This is apparent in figure, as the salt concentration in the Kaolin-NaCl solution increase the total conductance increases owing to the lower resistive parallel as a result of the pollution layer proposed in Figure 4-4 in section 4.3.1.

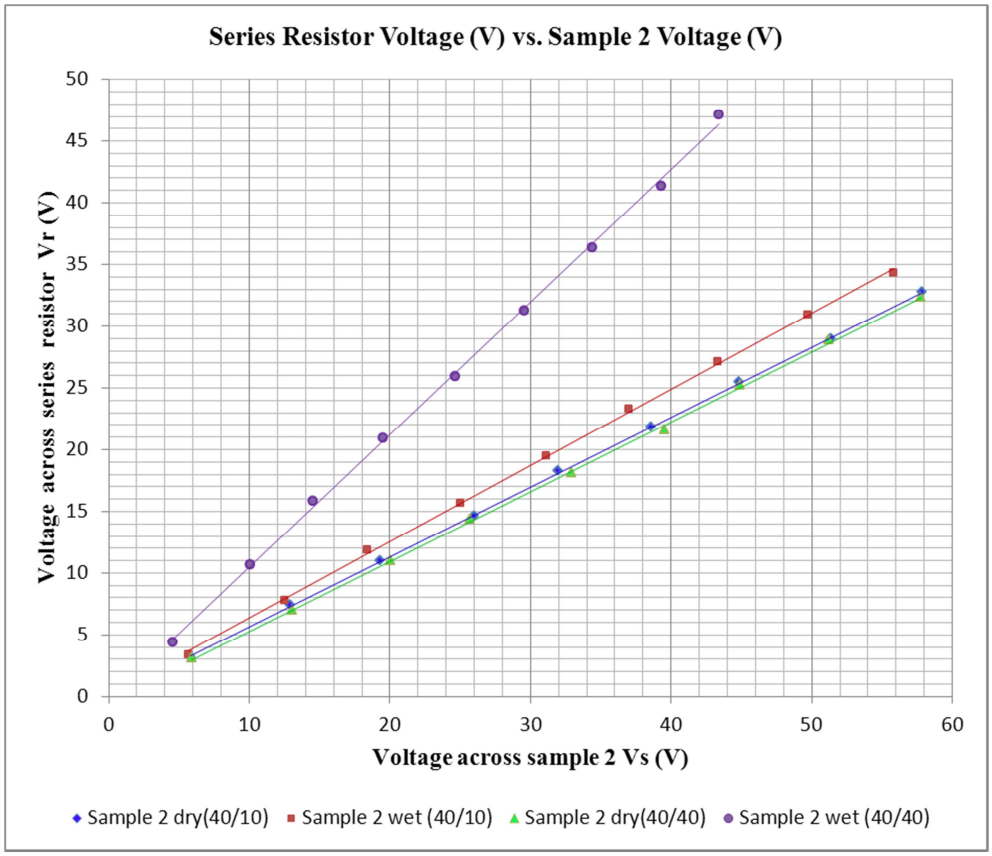


Figure 5-6: Voltage distribution across Sample 2 and series resistor for wet and dry pollution layer

A similar result to that of Figure 5-5 is observed with sample 2. This is expected, it was shown in the previous section that surface conductivity is a function of pollution severity and the form factor. It is independent of the size of the insulating surface. The two surfaces under test though of different sizes share the same form factor of 0.9 hence a similar results.

5.3.4 Conductivity test result analysis

From the results in Figure 5-5 and Figure 5-6 the pollution layer behave like and open circuit when the pollution is dry otherwise it offers a low resistive path. When the pollution layer is dry the voltage drop across the sample is therefore the total surface resistance R_{ST} is entirely due to the sample sheet surface resistance R_S whereas if the pollution layer is wet the resultant pollution R_{ST} is a parallel combination of R_S and pollution resistance R_P as shown in Figure 5-4.

If R, V_R and V_S are the series resistance, voltage across the series resistance and voltage across sample sheet respectively, then R_{ST} is given in equation 5-3.

$$R_{ST} = R\frac{V_S}{V_R} \qquad 5\text{-}3$$

If the pollution layer is dry, the total surface resistance R_{STdry} is given in equation 5-4.

$$R_{STdry} = R_S \qquad 5\text{-}4$$

Whereas if the pollution is wet, the total surface resistance R_{STwet} is given in equation 5-5.

$$R_{STwet} = \frac{R_S R_P}{R_S + R_P} \qquad 5\text{-}5$$

Solving for R_p in equation 5-4 and equation 5-5 then

$$R_P = \frac{R_S R_{STwet}}{R_S - R_{STwet}} \qquad 5\text{-}6$$

From equation 5-2 surface conductivity is given by equation 5-7

$$\sigma_S = \frac{1}{R_P} \times \frac{L}{W} \qquad 5\text{-}7$$

R_{ST} for both dry and wet conditions is obtained from the product of the series resistance and the gradient of either Figure 5-5 or Figure 5-6. The result is substituted in equation 5-6 to determine Rp. The resultant surface conductivity for the two samples polluted with the kaolin/ NaCl pollution concentration of 40 g/10 g per litre of distilled water is shown in table 5-2.

Table 5-2: Surface conductivity for sample sheets polluted with a Kaolin-NaCl solution with concentration of 40 g-10 g per litre of distilled water.

	$R_{STdry} = R_S$	$R_{STwet} = \frac{R_S R_P}{R_S + R_P}$	$R_P = \frac{R_S R_{STwet}}{R_S - R_{STwet}}$	$\sigma_S = \frac{1}{R_P} \times \frac{L}{W}$
Sample 1	5,880 (Ω)	5,230 (Ω)	46,980 (Ω)	19.6 (µS)
Sample 2	5,970 (Ω)	5,380 (Ω)	54,130 (Ω)	17.3 (µS)

According to 1EC 815 surface conductivity for light pollution severity lies between 15 µS and 20 µS. This confirms samples in Table 5-2 were lightly polluted and in turn the pollution severity on the insulated conductor covers under test.

When the similar analysis is repeated when the sample sheets are polluted with a solution having an increased salt concentration of 40 g per litre, the results shows that the pollution severity class increases as well. This is as expected since solution conductivity is proportional to the amount of salts in the pollutant.

5.3.5 Limitation of the test method

From conductivity measurement results above it was observed that pollution condensation plays a very important role in pollution classification when using the surface conductance measurement method. The right amount of pollution condensation needs to be achieved during the test at all times to give consistent reading otherwise the resultant conductivity encroaches into the adjacent class. A more accurate result is obtained by conducting the ESDD measurement. However severity pollution severity class have a defined range and the results in table 5-2 falls within that range.

5.4 Flashover stress and leakage current experimental results

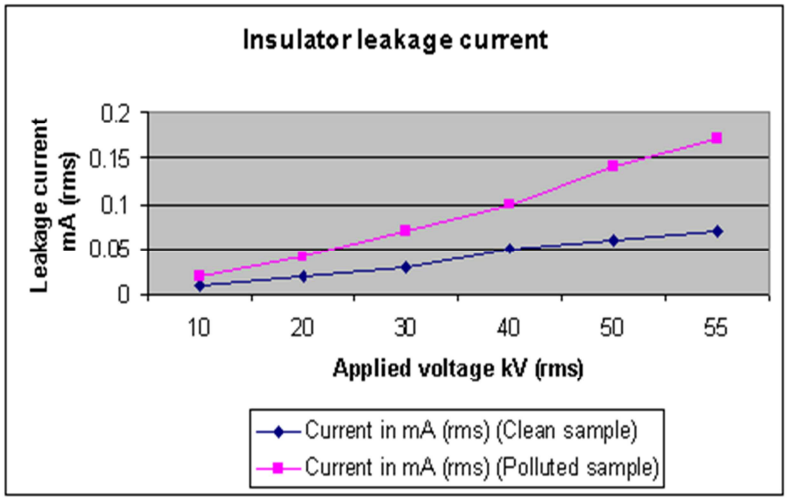


Figure 5-7: Leakage current on clean vs. polluted insulated conductor cover measured at position P1

From the test results in Figure 5-7, it is observed that the corresponding surface leakage current for a polluted insulated conductor cover is higher than that of a clean surface for all voltage levels measured. This is as anticipated since the pollution in its wet state reduces the surface resistance.

From the results in Table 5-2 it is observed that for the same pollution severity level, the leakage current increases as the contact position is varied from positions P1 to P3. Moreover as the position of the contact to earth is moved towards the live conductor end the withstand voltage stress reduces and flashover occurs.

Table 5-3: Voltage vs. Leakage current at different contact position along the insulator surface

Applied voltage in kV(rms)	**Creepage distance from the live insulated conductor cover end**		
	550mm	300mm	150mm
	Current in mA(rms) (polluted sample) Position 1	Current in mA(rms) (polluted sample) Position 2	Current in mA(rms) (polluted sample) Position 3
10	0.02	0.02	0.25
20	0.04	0.04	0.59
30	0.07	0.07	flashover
40	0.10	0.10	

50	0.14	0.14	
55	0.17	flashover	

The results in Table 5-2 are attributed to reduced creepage length that results in reduced surface resistance and currents above the critical values.

5.5 Discussion

The experimental results show that the leakage current for both the clean and polluted insulated conductor covers increases with increasing voltage. This is in agreement with similar findings in the literature [23]. The results also show that the leakage current on polluted insulated conductor covers is higher than on clean insulated conductor covers at corresponding contact positions. The experimental results confirm the theoretical predictions.

Changing the contact positions along the insulator cover gets to a point where flashover occurs. The position closest to the conductor gave the lowest flashover voltage. This is attributed to the reduced creepage distance along the insulator at that position and is in agreement with predictions by Verma [21]. Under the same conditions there exists a point along the insulator length where the leakage current reaches a critical flashover value, developing a critical flashover voltage which subsequently leads to flashover.

The critical values deduced experimentally (currents, voltages and specific creepage distance) are three times less than the theoretical predictions. This is attributed to the concentration of leakage current to a small surface area hence offering a higher resistance. A lower specific creepage of 5mm/kV is required for flashover to occur whereas on a high voltage insulator, a specific creepage distance of 16mm/kV is recommended.

5.6 Concluding remarks

The results confirm the theoretical predictions that a vulture on power lines can make contact with the insulated conductor cover at a position where critical

conditions are satisfied hence resulting in flashover. However the theoretical prediction (based on high voltage line insulator flashover theories) is 3 times more than the experimental results. This is attributed to the concentration of the leakage current on a small portion of the insulated conductor cover where contact with the vulture is made.

The insulated conductor cover flashover process is similar to that of high voltage line insulators. The only major difference is the concentration of the leakage current to a small portion of the insulated conductor cover surface area. To account for this difference a specific creepage distance lower than that required for high voltage line insulators should be specified to prevent flashover when there is contact with the vulture.

5.6.1 Accuracy of test results

The readings were measured several times and were repeatable within acceptable limits. The recorded variances were attributed to the varying pollution condensations which difficult to control since the tests were conducted in an open environment, this condition can potentially affect the accuracy of the reading, however the results could still give a good guide on choice of the appropriate dimension for the insulated conductor cover.

6 CONCLUSIONS

The research concludes that the insulated conductor cover design currently in use is susceptible to flashovers. When the vulture spans its wings so that the gap distance between the wing tip and a conductive pollution layer on the insulating conductor cover is less than 12 cm, sparkover across the gap occurs. If the insulated conductor cover surface is wet, surface flashover occurs at creepage distances less than 300 mm. Flashover can be mitigated by re-dimensioning or coating the insulated conductor cover with a silicone rubber layer. The latter is hydrophobic and less susceptible to pollution flashover by reducing the leakage currents below critical values.

Sparkover that occurs when the vulture comes in close proximity at distances less than 12 cm from the insulated conductor cover (with a conductive pollution layer) is because the cover is not screened. However if sparkover across the gap does occur, sufficient creepage length will reduce the magnitude of the leakage current flowing to earth through the vulture by providing a higher surface impedance path

The equivalent circuits used to model surface flashover on the insulated conductor cover are limited to predicting the initial condition of surface flashover for the worst case conditions. However the circuit allows the designer to simulate resultant leakage currents that enable selection of appropriate design for various surface conditions that prevent any condition that supports surface flashover.

Recommendation

To ensure the successful implementation of the insulated conductor cover for vulture electrocution it is recommended that:

- Hydrophobic insulation material should be used for the insulated conductor cover as it offers high surface insulation resistance even in the presence of moist pollution hence offering an improved creepage distance.

- The current insulated conductor cover in Figure 2-1 should be redesigned such that the outer ends that snugly fit to the conductor are of the same dimension as the middle section. This will improve the creepage length at the point of contact resulting in less probability of flashover.

- The proposed conductor corrosion test needs to be concluded, it has been hypothesised that humid conditions that may develop inside the insulated conductor cover can potentially cause corrosion of the enclosed portion of the conductor. These tests are expected to confirm that the life span of the conductor is not affected.

References

1. SAPP Environmental Sub-Committee, “The Management of Wildlife Interactions with Overhead Power Lines training manual”, African centre for energy and environment, 13 August 2003.
2. Chris van Rooyen, “Bird Impact Assessment”, Eskom Distribution Division Central Region, 2009
3. IEEE Task Force, “Preventative measures to reduce bird related power outages-part I: Electrocution and collision”, IEEE Transaction on Power Delivery. Vol 19 No. 4. pp. 1843-1847, October 2004.
4. R. Sundararajan (Chair), Member, IEEE, “Preventive Measures to Reduce Bird Related Power Outages-Part II: Streamers and Contamination”, IEEE Transactions on Power Delivery, Vol 19. No. 4, October 2004.
5. Tyco Electronics, “Insulation, Asset and Wildlife Protection selection guide”, Tyco Electronics Corporation, 2008.
6. Johan van Staden, Eskom Plant Performance, Personal communication
7. J.P. Holtzhausen, University of Cape Town, Personal communication.
8. IEC 60815:1996. “Guide for the Selection of Insulators in Respect Of Polluted Conditions”. IEC Recommendations. Publication.
9. http://www.oiseaux-birds.com/card-cape-vulture.html. Cited 10 December 2011.
10. Nelson, M.W, “Power lines progress report on eagle protection research” Idaho Power Company, Boise, Idaho, USA.1979.
11. Cigre Task Force 33.13.01 “Polluted Insulators: a review of current knowledge”, Cigre Task force, June 2000.
12. Reather H, Electron avalanches and electrical breakdown, Butterworth, 1964. X1

13. A Pedersen, “Calculation of spark breakdown voltage or corona starting voltages in non-uniform fields” IEE transactions on power apparatus and systems, Vol 2 pp200-205, February 1967.

14. N.L Allen, “Analysis and comparison of rod-plane and rod-rod gaps as direct voltage measurement devices”, IEE proceedings-A, Vol. 39.No. 6. November 1992

15. SANS 60060-1,“High-voltage test techniques Part 1: General definitions and test requirements”, 2011.

16. IEEE, “Standard Techniques for High-Voltage Testing”, IEEE Std 4-1995.

17. P.L. Bellaschi, “ Impulse and 60 cycle strength of air” AIEE electrical machinery, New York, November 1934

18. A. Jeffery, “Power frequency AC sparkover voltage measurements of small air gaps”, IEEE Transactions on Power delivery , Vol 14 No. 3, July 1999

19. F.A.M. Rizk, “Mathematical models for pollution flashover”, Electra no. 78 Technical papers.

20. J. Loberg E. Salthouse, “Dry-Band Growth on Polluted Insulation”, IEEE Transactions on electrical insulation, Vol. EI-6. No.3. September 1971

21. Verma M.P., “Mechanism of AC flashover on polluted insulator”, ISPPISD, Madras, 1981

22. Wilhelm H. Schwardt, “A comparison between measured leakage current and surface conductivity during salt fog tests”, Department of Electrical and Electronic engineering, University of Stellenbosch, South Africa

23. Waluyo, P.M. Pakpahan, Suwarno, “Study on the electrical equivalent circuit model on polluted outdoor insulators”,8th International Conference on Dielectrics, pp. 546 -549, 2006

24. S. Manjang, I. Abduh, “Leakage current pattern on artificially polluted Porcelain and Polymer insulators”, 8th International Conference on Dielectrics, pp. 443-446, 2006

25. Fabio Bologna, “The planning, design and construction of overhead power lines”, Crown Publications cc, South Africa, May 2010.

26. IEC 60507, “Artificial pollution tests on high-voltage insulators to be used on a.c. systems”, 1991

Bibliography

1. Rick Harness, “Raptor electrocution and distribution pole types”, North American Wood Pole Coalition technical bulletin, EDM International, Inc. Fort Collins, Colorado, October 2000.
2. Salam M.A. “Measurement of conductivity and equivalent salt Deposit of contaminated glass plate”, Department of Electrical and computer engineering, Sultan Qaboos University
3. A. Mohammad, A.Salman, “hydrophobicity of silicon rubber used for outdoor insulation (an overview)”, UET Taxila, Pakistan, 30 April 2007.
4. Waluyo, P.M. Pakpahan, Suwarno, ”Study on the electrical equivalent circuit model on polluted outdoor insulators”,8th International Conference on Dielectrics, pp. 546 -549, 2006
5. J. Chubb, “An introduction to electrostatic measurements”, John Chubb instrumentation Ltd, Cheltenham, 2007.
6. J.M Meek, J.D Craggs, “Electrical breakdown of gases”, Clarenden, 1953.
7. EPRI AC Transmission line reference book – 200kV and above third Edition. Chapter 8.
8. T. Bernstein, “Electrical shock hazards and safety standards”, IEEE transaction on education, Vol. 34. No. 3 August 1991.
9. ELEN 7007 Electrical discharges course notes, School of electrical and information Engineering, University of the Witwatersrand, Johannesburg 2009.
10. S. Manjang, I. Abduh, “Leakage current pattern on artificially polluted Porcelain and Polymer insulators”, 8th International Conference on Dielectrics, pp. 443-446, 2006.

11. N.L. Allen, “Dielectric Breakdown in non-uniform field air gaps”, IEEE Transactions on electrical insulation , Vol 28 No. 2, April 1993

12. P. Oterga, “Impulse breakdown voltage of air gaps: A new approach to atmospheric correction factors applicable to international standards”, IEEE transactions on dielectrics and Electrical insulation, Vol 14, No. 6, December 2007

Appendices

Insulated conductor cover Technical data

ASSET PROTECTION

Technical Data

Medium-Voltage Products*

Test and Performance Data

Material Properties	Test method	Requirements	BBIT BPTM	BCIC HVIS	CITM	BCAC, HVCE-WA, HVBT, OLIT	HVCE	MVLC	BISG RRBB
Electrical									
Volume resistivity	ASTM D-257, IEC 93	ohm-cm min.	1.0x1013	1.0x1013	1.0x1013	1.0x1013	1.0x1013	1x1013	1x1013
Dielectric constant	ASTM D-150, IEC 250	max.	5.0	5.0	5.0	5.0	5.0	5.0	5.0
Dielectric strength	ASTM D-149, IEC 243	V/mil at 1.3mm min.						550	
		V/mil at 1.5mm min.	500						
		V/mil at 2mm min.	450	330		330	250		
		V/mil at 2.5mm min.	400						380
		V/mil at 3mm min.	350		350				
Thermal									
Thermal endurance	IEEE 1-1969, IEC 216	min.	105°C	105°C	110°C	105°C**	110°C	105°C	
Accelerated aging for 168 hours	ISO 188	Tensile strength	1450 psi	1450 psi	2160 psi	1450 psi.	1100 psi	1450 psi	2450 psi
		Ultimate elongation	300%	300%	300%	300%	300%	100%	25%
		Aging Temp.	120°C	120°C	120°C	120°C	120°C	150°C	120°C
Chemical									
Flammability	ANSI C37.20	Pass	Pass	Pass		Pass			
Water absorption	ISO/R 62, procedure A	1% max. after 14 days at 23°C	Pass	Pass	Pass	Pass	Pass	Pass	Pass
Low-temperature flexibility	ASTM D-2671, procedure C	No cracking after 4 hr	Pass -40°C	Pass -40°C	Pass -40°C	Pass -40°C	Pass -40°C	Pass -20°C	Pass -40°C
Corrosion	Copper Mirror, ASTM D-2671, procedure B	Passed visual inspection after 16 hr		Pass 150°C		Pass 150°C		Pass 135°C	
Physical									
Tensile strength	ASTM D-638, ISO 37	psi. (min.)	1450 <4 mm, 1150 >4 mm	1450	2160	1450	1150	1450	2450
Ultimate elongation	ASTM D-638, ISO 37	% min.	300	300	400	300	300	200	25

Note: Blank spaces indicate that property was not measured during product qualification.
**Each product's voltage rating will be displayed with its selection information.*
***Properties measured on backing material only. HVBT and OLIT have a 70°C maximum continuous operating temperature limit.*

Low-Voltage Products

Test and Performance Data

Material properties	Test method	LVIT, LVBT, LVBC
Electrical		
Volume resistivity	ASTM D-257, IEC 93	1x1013 ohm-cm minimum
Dielectric constant	ASTM D-150, IEC 250	6.0 maximum
Dielectric strength	ASTM D-149, IEC 243	330 V/mil at 2.5 mm
Thermal		
Thermal endurance	IEEE 1-1969, IEC 216	105°C minimum
Accelerated aging	ISO 188	168 hr at 150°C
	Tensile strength	1600 psi minimum
	Ultimate elongation	200% minimum
Chemical		
Flammability	ICEA-S-19-81	Pass
Water absorption	ISO/R 62, procedure A	0.5% maximum after 14 days @ 23°C
Low-temperature flexibility	ASTM D-2671, procedure C	No cracking after 4 hr at -40°C
Physical		
Tensile strength	ASTM D-638, ISO 37	1750 psi minimum
Ultimate elongation	ASTM D-638, ISO 37	350% minimum

30

Rod-rod gap sparkover peak voltages [13]

Gap spacing (cm)	60 Hz (kV peak)	Critical sparkover (kV peak)			
		1.2 × 5 μs) wave (nonstandard)		(1.2 × 50 μs) wave	
		Positive	Negative	Positive	Negative
2	25	33	33	31	31
3	36	43	43	41	41
4	46	52	52	50	50
5	53	61	63	59	61
6	60	66	71	64	69
8	70	81	87	75–76*	84
10	79	96	104	87–91*	99
12	86	115	121	100–107*	116
14	95	134	138	114–125*	132
16	104	153	155	129–142*	147
18	112	170	171	139–153*	158
20	120	188	188	154–161*	176
25	143	234	232	184	217
30	167	277	274	217	249–260*
35	192	320	316	250	283–306*
40	218	362	358	281	313–348*
45	243	405	405	309	347–375*
50	270	445	449	339	382–392*
60	322	525	535	392	455
70	374	605	625	450	525
80	422	690	710	510	585
90	473	765	790	570	670